mediated by nonreceptor tyrosine kinase c-Abl, increasing its stability at protein level and proapoptotic activity (Agami *et al.*, 1999; Gong *et al.*, 1999). Alternatively, it has been shown that the prolyl isomerase Pin1 as well as the transcriptional coactivator Yes-associated protein YAP enhances p73 acetylation mediated by p300 in response to DNA damage, and thereby increasing p73 stability (Mantovani *et al.*, 2004; Strano *et al.*, 2005). These observations suggest that the stress-induced chemical modifications of p73 play a critical role in regulating p73 stability and activity. Accumulating evidence strongly suggests that p73 protein level is regulated in a ubiquitin-mediated proteasomal degradation pathway (Balint *et al.*, 1999; Lee and La Thangue, 1999; Bernassola *et al.*, 2004). Unlike p53, MDM2 binds to the NH_2-terminal transactivation domain of p73 and inhibits its transcriptional activity but does not target p73 for ubiquitin-mediated degradation (Balint *et al.*, 1999; Zeng *et al.*, 1999), implying that the protein stability of p73 is regulated through a pathway distinct from that of p53.

The activation of nuclear factor κB (NF-κB) has been shown to play an important role in the control of cell survival processes, which protects cells from a wide variety of apoptotic stresses (Beg and Baltimore, 1996; Van Antwerp *et al.*, 1996; Wang *et al.*, 1996, 1998). For example, camptothecin-mediated activation of NF-κB provides an antiapoptotic function (Huang *et al.*, 2000), and inhibition of NF-κB results in radiosensitization (Yamagishi *et al.*, 1997). Tumor necrosis factor alpha (TNF-α) activates the NF-κB-mediated cellular protective mechanism against the proapoptotic effect of TNF-α through the induction of the NF-κB-target genes that are involved in the inhibition of apoptosis (Beg and Baltimore, 1996; Van Antwerp *et al.*, 1996; Wang *et al.*, 1996). In addition to the antiapoptotic effect of NF-κB, NF-κB also contributes to cellular transformation and oncogenesis. Consistent with this notion, constitutive high levels of NF-κB activity were detectable in various human tumors (Bayon *et al.*, 2003). Intriguingly, Wan and DeGregori (2003) reported that NF-κB promotes T-cell survival in response to antigenic stimulation through the downregulation of p73; however, the precise molecular mechanism behind the NF-κB-mediated reduction of p73 is less well understood.

In the present study, we have found for the first time that NF-κB activation promotes the ubiquitin-dependent proteasomal turnover of p73, and the transcriptional activity of NF-κB is required for the NF-κB-mediated degradation of p73. Our present findings provide an evidence that NF-κB-mediated degradation of p73 might be a novel inhibitory mechanism of p73 function.

Results

Ectopic expression of NF-κB decreases p73α level

We first asked whether NF-κB could affect the expression level of proapoptotic p73. To this end, p53-deficient H1299 cells were co-transfected with the constant amount of the expression plasmid for FLAG-p73α together with or without the increasing amounts of the HA-p65 plus HA-p50 expression plasmids. At 48 h after transfection, whole-cell lysates were prepared, and immunoblot analysis revealed that the expression level of FLAG-p73α is significantly reduced in cells co-expressing HA-p65 and HA-p50 in a dose-dependent manner (Figure 1a). Under our experimental conditions, *p73α* mRNA level remained unchanged even in the presence of the exogenous HA-p65 and HA-p50. Similar results were also obtained in COS7 cells (Figure 1b). Next, we examined the effect of ectopically expressed NF-κB on the endogenous p73. COS7 cells were co-transfected with or without the increasing amounts of the expression plasmids encoding HA-p65 plus HA-p50. At 48 h after transfection, whole-cell lysates were immunoprecipitated with the normal mouse serum (NMS) or with the anti-p73 antibody, followed by immunoblotting with the anti-p73 antibody. As shown in Figure 1c and d, the endogenous p73α was significantly decreased at protein level in the presence of the ectopically expressed HA-p65 and HA-p50.

NF-κB specifically downregulates p73α

We tested whether NF-κB could reduce the expression levels of the other p53 family members including p53 and p63. Figure 2a shows the domain structures of p53, p73α, p73β and p63α. Whole-cell lysates prepared from H1299 cells transiently co-transfected with the indicated combinations of the expression plasmids were analysed for the expression levels of FLAG-p53, FLAG-p73β and p63α. In a sharp contrast to p73α, the enforced expression of NF-κB had marginal effects on the levels of FLAG-p53, FLAG-p73β and p63α (Figure 2b–d). Under our experimental conditions, NF-κB had undetectable effect on ΔNp73 (data not shown). These results strongly suggest that NF-κB-mediated downregulation is highly specific to p73α.

TNF-α-mediated activation of NF-κB results in a downregulation of the endogenous p73α

We sought to examine whether the activation of the endogenous NF-κB could affect the expression level of the endogenous p73. H1299 cells stably transfected with the NF-κB luciferase reporter plasmid (Muta and Takeshige, 2001) were treated with TNF-α as indicated, and their luciferase activity was determined. As shown in Figure 3a–c, TNF-α treatment enhanced the NF-κB-dependent transcriptional activation, and p65 as well as p50 translocated into cell nucleus in response to TNF-α as examined by immunoblotting and indirect immunofluorescence staining. As expected, immunoprecipitation experiments demonstrated that the expression level of the endogenous p73α protein is significantly reduced in response to TNF-α, whereas *p73α* mRNA level remained unchanged in cells exposed to TNF-α (Figure 3d). TNF-α treatment had no significant effects on the viability of cells (data not shown). These results suggest that the TNF-α-mediated activation of NF-κB leads to a

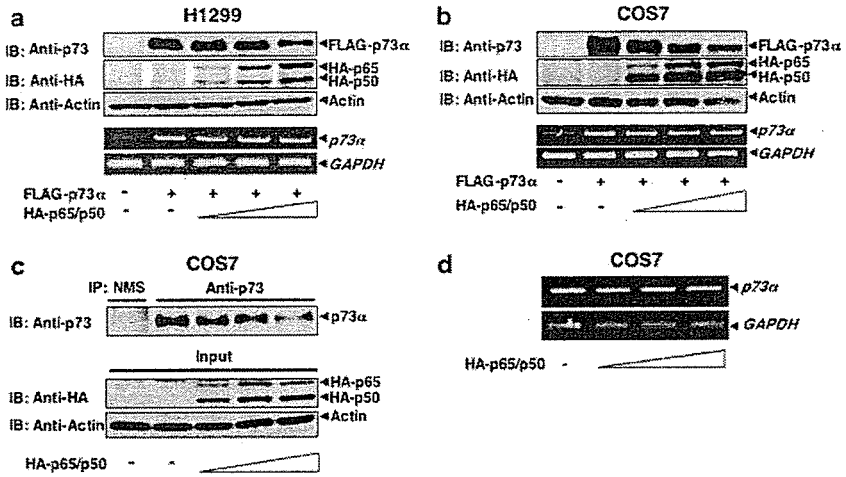

Figure 1 NF-κB decreases the amount of p73α. (**a** and **b**) Downregulation of p73α by NF-κB. H1299 (**a**) or COS7 (**b**) cells were co-transfected with the constant amount of the expression plasmid for FLAG-p73α (0.5 μg) together with or without the increasing amounts of the HA-p65 and HA-p50 expression plasmids (0.5, 1.0 and 1.5 μg). At 48 h after transfection, whole-cell lysates or total RNA were subjected to immunoblotting or RT–PCR analysis, respectively. Expression of FLAG-p73α, HA-p65 and HA-p50 was verified by the indicated antibodies. Actin was used to confirm that an equivalent amount of protein was loaded into each lane. For RT–PCR, ethidium bromide staining of *GAPDH* confirmed equivalent loading. (**c** and **d**) Downregulation of the endogenous p73α by the enforced expression of NF-κB. COS7 cells were co-transfected with or without the increasing amounts of HA-p65 and p50 expression plasmids. At 48 h after transfection, whole-cell lysates or total RNA were processed for the immunoprecipitation with the NMS or with the anti-p73 antibody, or subjected to RT–PCR, respectively.

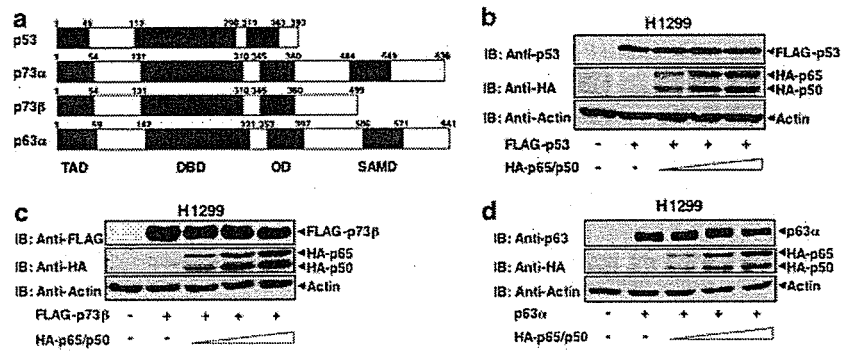

Figure 2 NF-κB-dependent downregulation is specific to p73α. (**a**) Domain structure of p53 family members. The transactivation domain (TAD), DNA-binding domain (DBD), oligomerization domain (OD), and SAM domain are indicated. (**b–d**) NF-κB does not affect the expression levels of p53, p73β and p63α. H1299 cells were co-transfected with the constant amount of the expression plasmid for FLAG-p53 (**b**), FLAG-p73β (**c**) or p63α (**d**) along with or without the increasing amounts of the expression plasmids for HA-p65 and HA-p50. At 48 h after transfection, whole-cell lysates were analysed by immunoblotting with the indicated antibodies. The *lower panels* show actin to demonstrate equal loading of the gels.

reduction in the amounts of proapoptotic p73α at protein level. In contrast to TNF-α, cisplatin treatment had negligible effects on the transcriptional activity of NF-κB, and immunoprecipitation experiments revealed that the endogenous p73α is induced to be accumulated in cells exposed to cisplatin (Supplementary Figure S1).

To confirm our hypothesis that the downregulation of p73α is dependent on NF-κB, we further investigated whether the expression level of the endogenous p73α could be altered in the absence of heterodimeric complex of NF-κB. To this end, we used mouse embryonic fibroblasts (MEFs) derived from p65 knockout mice (Figure 4a) (Beg *et al.*, 1995). Whole-cell lysates were prepared from p65 knockout and WT MEFs exposed to TNF-α (20 ng/ml) or left untreated. Immunoprecipitation experiments demonstrated that TNF-α-mediated reduction of the endogenous p73α is observed in WT MEFs but not in p65 knockout MEFs (Figure 4b and c), indicating that the presence of functional NF-κB complex is required for the downregulation of p73α.

NF-κB stimulates the ubiquitin-dependent proteasomal degradation of p73α

To determine whether NF-kB could modulate p73α turnover, we sought to examine the half-life of p73α in the presence or absence of the exogenously expressed NF-κB using cycloheximide blockade. COS7 cells were

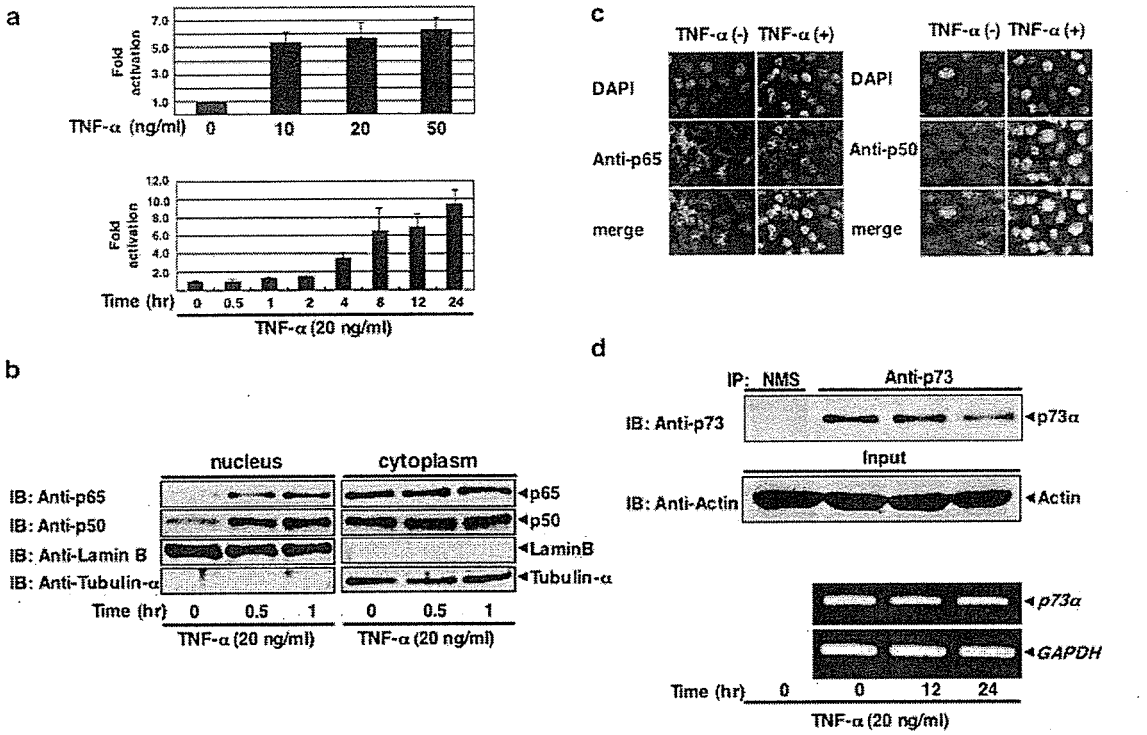

Figure 3 TNF-α treatment causes a downregulation of the endogenous p73α. (a) TNF-α treatment enhances the transcriptional activity of NF-κB. H1299 cells stably transfected with the luciferase reporter plasmid carrying 1xκB site and *Renilla* luciferase construct were exposed to the indicated concentrations of TNF-α for 24 h (upper panel) or treated with 20 ng/ml of TNF-α for the indicated time periods (lower panel). At the indicated time periods after the treatment with TNF-α, luciferase assays were performed. (b and c) Nuclear translocation of p65 and p50 in response to TNF-α. H1299 cells exposed to TNF-α (20 ng/ml) for the indicated time periods were separated into nuclear and cytoplasmic fractions. The aliquots of these fractions were analysed by immunoblotting with the anti-p65 (1st panel) or with the anti-p50 (2nd panel) antibody. These fractions were also analysed for nucleus-specific Lamin B (3rd panel) and cytoplasm-specific α-tubulin (4th panel) to show the validity of our fractionation technique (b). H1299 cells were treated with TNF-α (20 ng/ml) for 1 h or left untreated. Cells were fixed and then incubated with the anti-p65 (left panels) or with the anti-p50 (right panels) antibody. Cell nuclei were stained by DAPI. Cellular localization was detected by fluorescence microscopy. The merged images indicate the nuclear translocation of p65 and p50 in response to TNF-α (c). (d) TNF-α treatment decreases the expression level of the endogenous p73α. H1299 cells were treated with TNF-α (20 ng/ml) for the indicated time periods or left untreated. Whole-cell lysates or total RNA were subjected to immunoprecipitation with the indicated antibodies or RT–PCR, respectively.

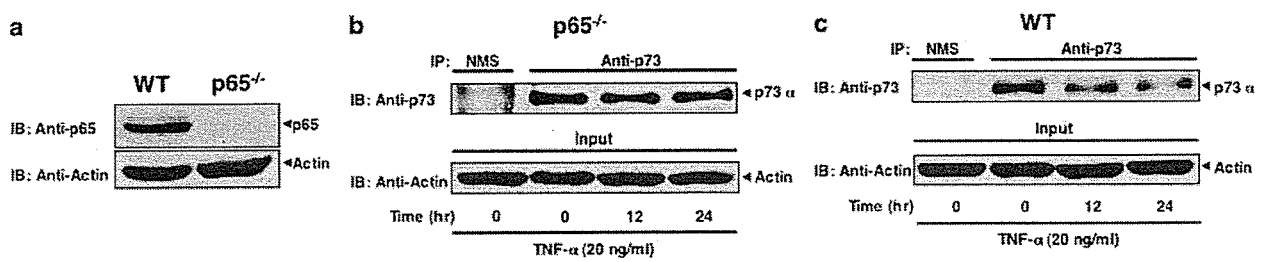

Figure 4 NF-κB-dependent reduction of p73 in response to TNF-α. (a) Expression of the endogenous p65 in MEFs. Whole-cell lysates from WT and p65 knockout MEFs were analysed for p65 by immunoblotting. (b and c) TNF-α-dependent downregulation of the endogenous p73α is observed in WT but not in p65 knockout MEFs. p65 knockout (b) and WT (c) MEFs were treated with TNF-α (20 ng/ml) for indicated time periods or left untreated. Whole-cell lysates were subjected to immunoprecipitation with NMS or with the anti-p73 antibody, followed by immunoblotting with the anti-p73 antibody.

co-transfected with the constant amount of the expression plasmid for FLAG-p73α along with or without the constant amount of the expression plasmids encoding HA-p65 and HA-p50. At 24 h after transfection, cells were exposed to cycloheximide (100 μg/ml). At the indicated time points, whole-cell lysates were subjected to immunoblotting with the anti-p73 antibody. Consistent with the previous observations (Lee and La Thangue, 1999), transiently expressed FLAG-p73α had a half-life of about 3 h (Figure 5a). When FLAG-p73α was co-expressed with HA-p65 and HA-p50, the degradation rate of FLAG-p73α was faster than that

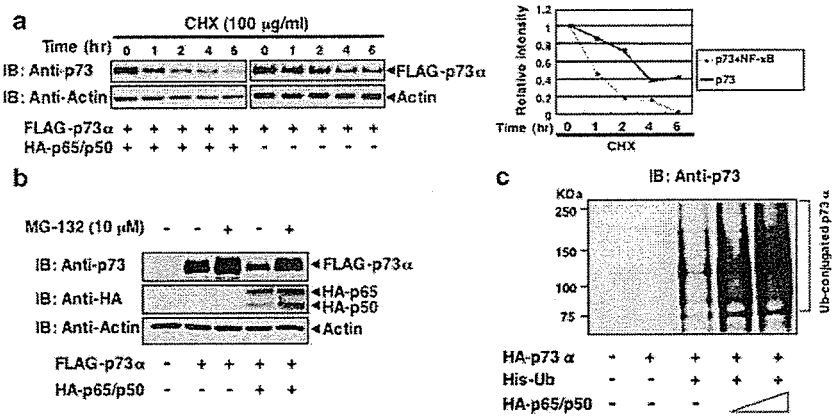

Figure 5 NF-κB-induced reduction of p73 is regulated by a ubiquitin–proteasome pathway. (a) NF-κB decreases a half-life of p73α. COS7 cells were co-transfected with the constant amount of the FLAG-p73α expression plasmid together with or without the expression plasmids for HA-p65 and HA-p50. At 24 h after transfection, cells were exposed to cycloheximide (100 μg/ml). At the indicated time points after the addition of cycloheximide, whole-cell lysates were analysed for FLAG-p73α by immunoblotting. Actin was used for equal protein loading. Densitometry was used to quantify the amounts of FLAG-p73α, which normalized to actin. (b) NF-κB-mediated degradation of p73α is blocked by proteasomal inhibitor. COS7 cells were transfected either with FLAG-p73α alone or with FLAG-p73α, HA-p65 and HA-p50. At 40 h after transfection, cells were treated with or without MG-132 (10 μM) for 6 h. Whole-cell lysates were subjected to immunoblotting with the anti-p73, anti-HA or with anti-actin antibody. (c) NF-κB increases the ubiquitination levels of p73. COS7 cells were co-transfected with the constant amount of the expression plasmids for HA-p73α and His-Ub together with or without the increasing amounts of the HA-p65 and HA-p50 expression plasmids. At 40 h post-transfection, cells were treated with MG-132 (10 μM) for 6 h. Whole-cell lysates were then prepared, and ubiquitinated materials were recovered by Ni^{2+}-NTA-agarose beads, followed by immunoblotting with the anti-p73 antibody.

in cells expressing FLAG-p73α alone (a half-life of about 1 h). In addition, NF-κB had undetectable effects on the half-life of ΔNp73 (data not shown).

According to the previous reports (Balint *et al*., 1999; Lee and La Thangue, 1999; Bernassola *et al*., 2004), p73 protein level is regulated through the ubiquitin-mediated proteasomal degradation pathway. We then determined the effects of proteasomal inhibitor MG-132 on the expression level of p73α. As expected, proteasome inhibition resulted in a stabilization of FLAG-p73α (Figure 5b). Of note, the addition of MG-132 blocked the NF-κB-mediated degradation of FLAG-p73α, indicating that NF-κB-mediated degradation of p73α is regulated at least in part through the proteasomal pathway. To ask whether NF-κB could affect the ubiquitination levels of p73α, COS7 cells were co-transfected with the constant amount of the HA-p73α expression plasmid and the expression plasmid for His-tagged ubiquitin together with or without the increasing amounts of the expression plasmids for HA-p65 and HA-p50. After the treatment with MG-132 for 6 h, whole-cell lysates were prepared, and the ubiquitinated materials were recovered with Ni^{2+}-agarose beads followed by immunoblotting with the anti-p73 antibody. As shown in Figure 5c, ubiquitin-conjugated p73α was significantly increased upon the co-expression of HA-p73α with HA-p65 and HA-p50. Thus, it is likely that NF-κB mediates the ubiquitin-dependent proteasomal turnover of p73α.

NF-κB inhibits the transcriptional activity of p73α but not of p53

To evaluate whether NF-κB could influence the transcriptional activity of p73α, H1299 cells were co-transfected with the constant amount of the expression plasmid for FLAG-p73α, and the luciferase reporter construct controlled by the p53/p73-responsive element from the *BAX* or *MDM2* promoter together with or without the increasing amounts of the expression plasmids for HA-p65 and HA-p50. At 48 h after transfection, the luciferase activities were measured. As shown in Figure 6a, co-expression of FLAG-p73α with HA-p65 and HA-p50 significantly reduced the p73α-mediated transcriptional activation of *BAX* and *MDM2* promoters in a dose-dependent manner, and HA-p65 and HA-p50 had negligible effects on the reporter gene activities. Consistent with these results, RT–PCR analysis revealed that enforced expression of HA-p65 and HA-p50 inhibits the p73α-mediated transactivation of the endogenous *BAX*. In contrast, p53-mediated transcriptional activation was not affected in cells co-transfected with the HA-p65 and HA-p50 expression plasmids (Figure 6b).

NF-κB inhibits the proapoptotic activity of p73α

To further confirm the inhibitory effects of NF-κB on the p73 function, we examined the possible effects of NF-κB on the proapoptotic activity of p73α. H1299 cells were co-transfected with the indicated combinations of the expression plasmids. At 48 h after the transfection, cells were fixed, stained with propidium iodide, and the numbers of cells with sub-G1 DNA content were measured. In accordance with the previous report (Jost *et al*., 1997), expression of FLAG-p73α resulted in an increase in number of cells with sub-G1 DNA content (Figure 6c). Co-expression of FLAG-p73α with HA-p65 and HA-p50 decreased number of cells with sub-G1 DNA content in a dose-dependent manner. Additionally,

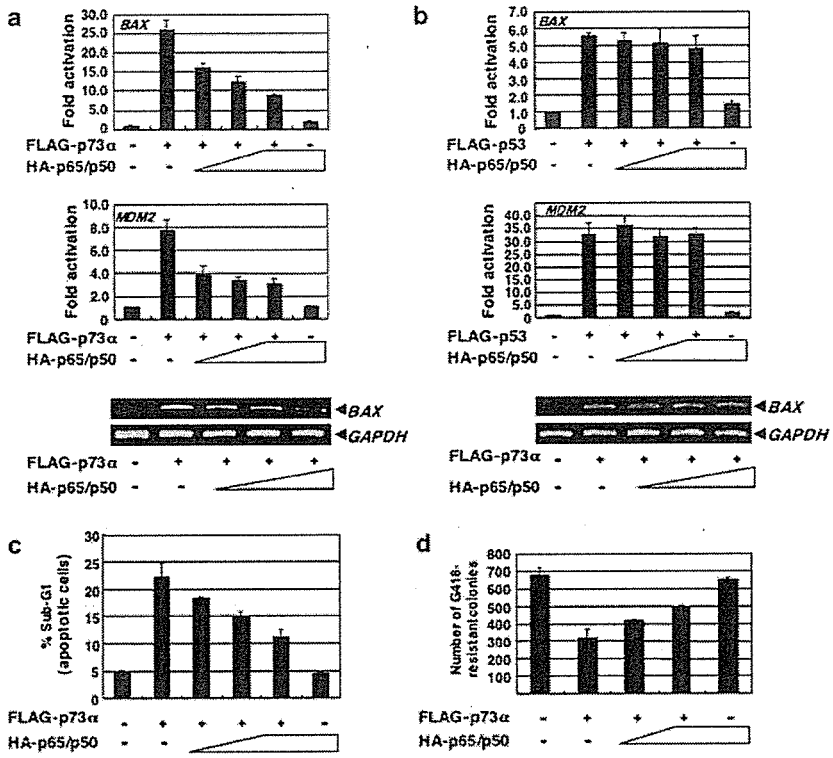

Figure 6 NF-κB inhibits the transcriptional as well as proapoptotic activity of p73. (**a** and **b**) NF-κB-mediated inhibition of the p73α-dependent transactivation but not of p53. H1299 cells were co-transfected with 25 ng of the expression plasmid for FLAG-p73α (**a**) or FLAG-p53 (**b**) together with 100 ng of the luciferase reporter construct, which carries the p53/p73-responsive element derived from *BAX* or *MDM2* promoter and 10 ng of the *Renilla* luciferase plasmid (pRL-TK) in the presence or absence of the increasing amounts of HA-p65 and HA-p50 expression plasmids (50, 100, or 200 ng). All transfections were performed in triplicate. At 48 h after transfection, cells were analysed for their luciferase activities. Firefly luminescence signal was normalized based on the *Renilla* luminescence signal. Results were shown as fold induction of the firefly luciferase activity compared with control cells transfected with the empty plasmid alone. For RT–PCR analysis, H1299 cells were co-transfected with the FLAG-p73α or FLAG-p53 expression plasmid together with or without the increasing amounts of the HA-p65 and HA-p50 expression plasmids. At 48 h post-transfection, total RNA was subjected to RT–PCR analysis for the expression of *BAX*. Amplification of *GAPDH* serves as an internal control. (**c**) FACS analysis. H1299 cells were co-transfected with the constant amount of the expression plasmid encoding FLAG-p73α together with or without the increasing amounts of the HA-p65 and HA-p50 expression plasmids. At 48 h after transfection, cells were fixed and stained with propidium iodide. (**d**) Colony formation assay. H1299 cells were co-transfected with the indicated combinations of the expression plasmids. At 24 h after transfection, cells were selected with G418 (400 μg/ml) for 2 weeks. The number of G418-resistant colonies was scored.

colony formation assays demonstrated that co-expression of FLAG-p73α with the increasing amounts of the HA-p65 and HA-p50 increases number of G418-resistant colonies as compared with that in cells expressing FLAG-p73α alone (Figure 6d). Taken together, these results strongly suggest that NF-κB has an ability to inhibit the transcriptional activity as well as proapoptotic function of p73α.

NF-κB does not bind to p73α in cells

To investigate how NF-κB decreases the stability and activity of p73α, we examined whether NF-κB could bind to p73α. H1299 cells were co-transfected with the indicated combinations of the expression plasmids. At 48 h after transfection, whole-cell lysates were immunoprecipitated with the anti-FLAG or anti-HA antibody followed by immunoblotting with the anti-HA or anti-p73 antibody, respectively. As shown in Figure 7a, the anti-FLAG immunoprecipitates did not contain HA-p65 and HA-p50. Similarly, FLAG-p73α was not co-immunoprecipitated with HA-p65 and HA-p50 (Figure 7b). Under our experimental conditions, FLAG-p73α was co-immunoprecipitated with MDM2 (data not shown), which was consistent with the previous reports (Balint *et al*., 1999; Zeng *et al*., 1999). Thus, it is likely that NF-κB-mediated inhibitory effects on p73α might be indirect without a direct interaction between them.

Transactivation function of NF-κB is required for the downregulation of p73α

To determine the molecular mechanism by which NF-κB contributes to the degradation of p73α, we focused on the COOH-terminal transactivation domain of p65 (Figure 7c). We generated a deletion mutant of p65 (HA-p65ΔC), which retains a nuclear localization signal but lacks a COOH-terminal transactivation domain. To assess the transactivation function of p65ΔC, we

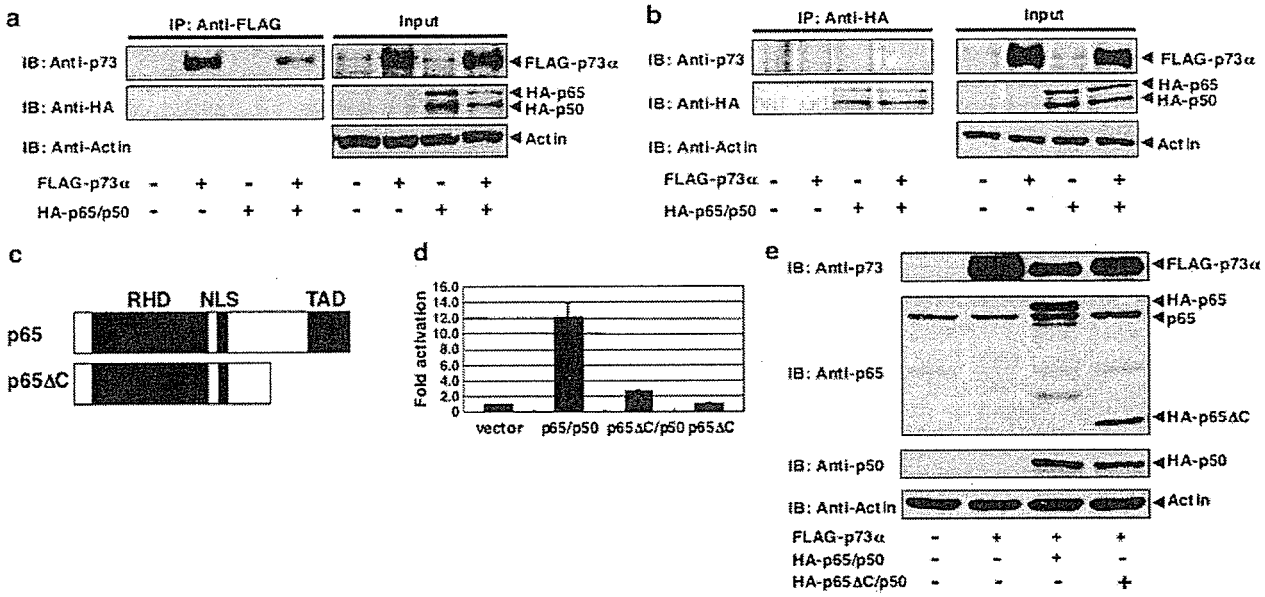

Figure 7 Transcriptional activity of NF-κB is required for the down regulation of p73. (**a** and **b**) Immunoprecipitation experiments. H1299 cells were co-transfected with the indicated combinations of the expression plasmids. At 48 h after transfection, whole-cell lysates were immunoprecipitated with the anti-FLAG (**a**) or with anti-HA (**b**) antibody, followed by immunoblotting with the indicated antibodies. Aliquots of whole-cell lysates were subjected to immunoblotting with the anti-FLAG or with the anti-HA antibody to monitor the expression levels of FLAG-p73α, HA-p65 and HA-p50 (right panels). (**c**) Schematic drawing of the full-length p65 and the COOH-terminal deletion mutant, p65ΔC. RHD, Rel homology domain; NLS, nuclear localization signal; TAD, transactivation domain. (**d**) p65ΔC lacks the transcriptional activity. H1299 cells were co-transfected with the NF-κB-responsive luciferase reporter plasmid and pRL-TK *Renilla* luciferase cDNA together with the empty plasmid, HA-p65 plus HA-p50, HA-p65ΔC plus HA-p50 or HA-p65ΔC. At 48 h after transfection, the luciferase activities were measured. (**e**) Downregulation of p73α is induced by the full-length p65 but not by p65ΔC. H1299 cells were co-transfected with the expression plasmid for FLAG-p73α together with HA-p65 plus HA-p50 or HA-p65ΔC plus HA-p50. At 48 h post-transfection, whole-cell lysates were processed for immunoblotting with the indicated antibodies. Actin was used to confirm that an equivalent amount of protein was loaded into each lane.

performed the luciferase reporter assay. As shown in Figure 7d, HA-p65ΔC alone failed to drive transcription from the NF-κB luciferase reporter, whereas two- to three-fold increase in the luciferase activity was detectable in cells expressing exogenous HA-p65ΔC and HA-p50, which might be due to the complex formation between the endogenous p65 and HA-p50. We then examined the possible effects of HA-p65ΔC on the expression level of FLAG-p73α. H1299 cells were co-transfected with the indicated combinations of the expression plasmids, and whole-cell lysates were analysed for the expression level of FLAG-p73α by immunoblotting. As shown in Figure 7e, WT p65 significantly reduced the amount of FLAG-p73α, whereas HA-p65ΔC had an ability to stabilize FLAG-p73α. Collectively, these results strongly suggest that the transactivation property of NF-κB is required for the degradation of p73α.

Discussion

In the present study, we have found for the first time that NF-κB promotes the ubiquitin-dependent proteasomal turnover of p73 in the absence of a direct physical interaction between them, and also demonstrated that the transcriptional activity of NF-κB is required for this process. In contrast, NF-κB had negligible effects on p53 and p63. Thus, it is likely that the NF-κB-mediated degradation of p73 contributes to the protection of cells from p73-dependent apoptosis. To our knowledge, this is the first report describing the detailed properties of the NF-κB-dependent inhibitory mechanism of p73 function.

Genotoxic stresses increase the stability of p73 and enhance its proapoptotic activity in a pathway dependent on c-Abl (Agami *et al*., 1999; Gong *et al*., 1999; Yuan *et al*., 1999). Intriguingly, Kawai *et al*. (2002) reported that c-Abl phosphorylates IκBα at Tyr-305 to increase its stability, and thereby inhibiting the nuclear translocation and activation of NF-κB, suggesting that the inactivation of NF-κB contributes to the c-Abl-mediated apoptosis. Additionally, it has been demonstrated that, during the cisplatin-mediated apoptosis in hepatocellular carcinoma cells, the downregulation of NF-κB transcriptional activity is correlated with the accumulation of p73 (Kim *et al*., 2004). In contrast to the DNA-damaging agents that activate c-Abl, TNF-α treatment had undetectable effect on c-Abl (Kharbanda *et al*., 1995). According to our present results, the activation of the endogenous NF-κB induced by TNF-α resulted in a significant decrease in the stability of p73α. Taken together, it is likely that c-Abl plays an important role in the regulation of NF-κB-mediated destabilization of p73.

Since we could not detect the physical interaction between NF-κB and p73α, NF-κB might regulate p73α stability through an indirect mechanism. Deletion analysis revealed that p65ΔC fails to reduce the amount of p73α, raising a possibility that the transactivation function of NF-κB might be required for the degradation of p73α, and that there could exist an unidentified E3 ubiquitin ligase(s) among the direct targets of NF-κB. Recently, Rossi *et al.* (2005) described that an HECT-type E3 ubiquitin ligase Itch binds to p73, and promotes its degradation through the ubiquitin–proteasome pathway. In contrast, Itch had no detectable effect on p53. Additionally, it has been shown that Jun kinase regulates the TNF-α-mediated apoptosis through the activation of Itch (Chang *et al.*, 2006). Although the examination of the human *Itch* promoter region showed the presence of several putative DNA-binding sites of NF-κB, the enforced expression of NF-κB or TNF-α-mediated activation of the endogenous NF-κB failed to induce the endogenous *Itch* as examined by RT–PCR (data not shown). Considering that p53 is targeted for ubiquitination not only by MDM2 but also by Pirh2 (Leng *et al.*, 2003), it is likely that an as yet unidentified E3 ubiquitin ligase(s) distinct from Itch might be involved in the NF-κB-mediated degradation of p73α.

Among p53 family members, the NF-κB-mediated reduction was highly specific to p73α. The protein stability of p53, p73β and p63α was unaffected by the enforced expression of NF-κB. Lee and La Thangue (1999) described that p73β is much more stable than p73α, suggesting that the unique COOH-terminal extension of p73α is critical for its stability. Recently, we found that RanBPM binds to the extreme COOH-terminal region of p73α to inhibit its ubiquitination and thereby increasing its stability (Kramer *et al.*, 2005). However, RanBPM had undetectable effects on the stability of p53. Thus, it is possible that RanBPM might mask the p73α COOH-terminal lysine residues, which could be sites for ubiquitin ligation. Alternatively, the unique p73α COOH-terminal region could mediate the interaction with unknown cellular protein(s) required for the degradation of p73 induced by NF-κB. Of note, Wan and DeGregori (2003) found that NF-κB promotes T-cell survival by inhibiting the activation of p73 in response to antigenic stimulation. They described that NF-κB directly antagonizes the E2F-1-dependent upregulation of *p73* transcription. The interpretation that NF-κB inhibits the transcription of *p73* is contradicted by our present findings. In addition to the DNA-damage-induced stabilization of p73, p73 is regulated at mRNA level in response to certain apoptotic and differentiation stimuli. For example, p73 is transcriptionally induced by E2F-1 during the apoptotic response to T-cell receptor activation (Lissy *et al.*, 2000). Fontemaggi *et al.* (2001) found that *p73* mRNA is upregulated by E2F-1 during muscle, neuronal and monocytic differentiation. Therefore, it appears that employment of the NF-κB-dependent transcriptional or post-translational mechanism to downregulate p73 is dependent upon the types of stimulation and/or cell types. The propensity of cells to survive or die is determined by the balance between proapoptotic and prosurvival signals. In this connection, NF-κB-mediated degradation of p73 is a novel mechanism that regulates cell survival and death in response to a variety of cellular stresses.

Materials and methods

Cell culture and transfection

MEFs, and COS7 cells were grown in Dulbecco's modified Eagle's medium supplemented with 10% heat-inactivated fetal bovine serum (Invitrogen, Grand Island, NY, USA), 100 IU/ml penicillin and 100 μg/ml streptomycin. p53-deficient human lung carcinoma H1299 cells were cultured in RPMI 1640 medium supplemented with 10% heat-inactivated fetal bovine serum and antibiotic mixture. Cultures were maintained at 37°C in a water-saturated atmosphere of 5% CO_2 in air. For transfection, H1299 and COS7 cells were transfected with the indicated combinations of the expression plasmids using LipofectAMINE 2000 (Invitrogen) and FuGENE6 (Roche Molecular Biochemicals, Indianapolis, IN, USA), respectively.

Construction of the deletion mutant of p65

p65ΔC was generated by PCR-based strategy using the forward primer 5′-TAGAATTCGGGACGATCTGTTTCCC CTCATC-3′ and the reverse primer 5′-TTCTCGAGTTAAA GGACTGGGGCAGAGGACGG-3′. Underlined nucleotides were *Eco*RI and *Xho*I restriction sites. Amplified fragments were digested with *Eco*RI and *Xho*I, and subcloned into the identical restriction sites of pCMV-HA expression plasmid (Clontech Laboratories, Palo Alto, CA, USA) to give pCMV-HA-p65ΔC.

Immunoblotting

Cells were washed twice with phosphate-buffered saline (PBS), lysed in buffer containing 25 mM Tris-Cl, pH 8.0, 137 mM NaCl, 2.7 mM KCl, 1% Triton X-100 and protease inhibitor cocktail (Sigma Chemical Co., St Louis, MO, USA), and sonicated for 10 s followed by centrifugation at 15 000 r.p.m. for 10 min at 4°C to remove insoluble materials. Aliquots of whole-cell lysates (25–50 μg) were boiled in the SDS-sample buffer for 5 min, loaded onto 8% SDS–PAGE, and electrotransferred onto Immobilon-P membranes (Millipore, Bedford, MA, USA). The membranes were blocked with TBS-T (50 mM Tris-Cl, pH 8.0, 100 mM NaCl and 0.1% Tween-20) containing 5% nonfat dry milk, and then incubated at room temperature for 1 h with the monoclonal anti-FLAG (M2, Sigma Chemical Co.), monoclonal anti-HA (12CA5, Roche Molecular Biochemicals), monoclonal anti-p73 (Ab-4, NeoMarkers, Inc., Fremont, CA, USA), monoclonal anti-p53 (PAb1801, Santa Cruz Biotechnologies, Santa Cruz, CA, USA), monoclonal anti-p63 (Ab-1, NeoMarkers), polyclonal anti-p65 (C-20, Santa Cruz Biotechnologies), polyclonal anti-p50 (H-119, Santa Cruz Biotechnologies), or with polyclonal anti-actin (20–33, Sigma Chemical Co.) antibody, followed by an incubation with corresponding horseradish peroxidase-conjugated goat anti-mouse or anti-rabbit secondary antibody (Cell Signaling, Beverly, MA, USA) for 1 h at room temperature. Protein bands were finally detected by enhanced chemiluminescence detection system (Amersham Biosciences, Inc., Piscataway, NJ, USA).

Co-immunoprecipitation analysis
Equal amounts of whole-cell lysates were precleared with 30 μl of protein G-Sepharose (Amersham Bioscience). After centrifugation, the supernatant was incubated with the indicated antibodies at 4°C for 2 h. The immunocomplexes were then incubated with protein G-Sepharose beads at 4°C for 1 h, which were then pelleted by centrifugation at 15 000 r.p.m. for 5 min. The immunocomplexes were washed with the lysis buffer three times at 4°C, denatured with an equal volume of 2 × SDS-sample buffer, and analysed by immunoblotting with the desired primary antibodies.

RT–PCR
Total RNA was prepared by using RNeasy Mini Kit (Qiagen Inc., Valencia, CA, USA) according to the manufacturer's protocol. One microgram of total RNA was used to synthesize the first strand cDNA using random primers and a SuperScript II reverse transcriptase (Invitrogen). Reverse transcription was performed at 42°C for 1 h, and the reverse transcripts were amplified by standard PCR with rTaq DNA polymerase (Takara, Ohtsu, Japan). The primers used for PCR were as follows: *BAX*, 5′-TTTGCTTCAGGGTTTCATCC-3′ (sense) and 5′-CAGTTGAAGTTGCCGTCAGA-3′ (antisense); *GAPDH*, 5′-ACCTGACCTGCCGTCTAGAA-3′ (sense) and 5′-TCCACCACCCTGTTGCTGTA-3′ (antisense); *p73α*, 5′-TGGAACCAGACAGCACCTACTTCG-3′ (sense) and 5′-TGCTGGAAAGTGACCTCAAAGTGG-3′ (antisense).

Subcellular fractionation
Cells were washed twice with PBS, lysed in lysis buffer containing 10 mM Tris-HCl, pH 7.5, 1 mM EDTA, 0.5% Nonidet P-40, and protease inhibitor cocktail for 10 min at 4°C, and centrifuged at 3000 r.p.m. for 5 min at 4°C to separate the soluble (cytoplasmic) from the insoluble (nuclear) fraction. The insoluble fraction was washed completely with the lysis buffer and resuspended in buffer containing 25 mM Tris-Cl, pH 8.0, 137 mM NaCl, 2.7 mM KCl, 1% Triton X-100 and protease inhibitor cocktail. The nuclear and cytoplasmic fractions were then analysed by immunoblotting with monoclonal anti-Lamin B (Ab-1, Oncogene Reseach Products), or with monoclonal anti-α-tubulin antibody (Ab-2, NeoMarkers, Inc.).

Indirect immunofluorescence assay
H1299 cells were seeded onto the glass coverslips, and treated with TNF-α (20 ng/ml) or left untreated for 1 h cells were then fixed with 3.7% formaldehyde for 30 min at room temperature, and permeabilized with 0.2% Triton X-100 for 5 min at room temperature. After cells were blocked with 3% bovine serum albumin (BSA) for 1 h at room temperature, they were incubated with the polyclonal anti-p65 or with the polyclonal anti-p50 antibody for 1 h at room temperature. The primary antibodies were detected with FITC-conjugated secondary antibody (Invitrogen) for 1 h at room temperature. Cell nuclei were stained with 4′6-diamino-2-phenylindole (DAPI) (Sigma Chemical Co.), and cells were observed under a Fluoview laser scanning confocal microscope (Olympus, Tokyo, Japan).

Luciferase reporter assay
H1299 cells were co-transfected with 100 ng of the p53/p73-responsive luciferase reporter plasmid (*BAX* or *MDM2*), 10 ng of pRL-TK *Renilla* luciferase cDNA, and 25 ng of the expression plasmid for FLAG-p73α or FLAG-p53 together with or without the increasing amounts of HA-p65 and HA-p50 expression plasmids. At 48 h after transfection, cells were washed with PBS, and resuspended in passive lysis buffer (Promega Corp., Madison, WI, USA). Both firefly and *Renilla* luciferase activities were assayed with the dual-luciferase reporter assay system (Promega Corp.). The firefly luminescence signal was normalized based on the Renilla luminescence signal.

Protein decay rate analysis
COS7 cells were co-transfected with the indicated combinations of the expression plasmids. At 24 h after transfection, cells were treated with cycloheximide (Sigma Chemical Co.) at a final concentration of 100 μg/ml. At the indicated time points after the treatment with cycloheximide, cells were harvested, and whole-cell lysates were processed for immunoblot analysis with the anti-p73 or with the anti-actin antibody. Densitometry was used to quantify the amounts of FLAG-p73α which normalized to actin.

Ubiquitination assay
COS7 cells were co-transfected with the constant amount of FLAG-p73α and His-tagged ubiquitin, together with or without the increasing amounts of HA-p65 and HA-p50. At 48 h after transfection, cells were exposed to MG-132 (20 μM) for 6 h. Cells were then lysed in lysis buffer containing 6 M guanidine–HCl, 0.1 M Na_2HPO_4/NaH_2PO_4, pH 8.0 and 10 mM imidazole. Ubiquitinated materials were recovered by Ni^{2+}-NTA-agarose beads (Qiagen), and subsequently analysed by immunoblotting with the anti-p73 antibody.

FACS analysis
H1299 cells were co-transfected with indicated combinations of the expression plasmids. At 48 h after transfection, cells were washed twice with PBS, resuspended in 600 μl of a propidium iodide mixture containing 0.05% RNase, 0.25% Triton X-100 and 50 μg/ml of propidium iodide, and then incubated in the dark at 4°C for 30 min. Prior to performing FACS analysis, cells were filtered through a 40-μm nylon mesh. Cells were then analysed using the FACScan system (Becton Dickinson, Mountain View, CA, USA) in conjunction with CellQuest software (Becton Dickinson).

Colony formation assay
H1299 cells were co-transfected with indicated combinations of the expression plasmids. Total amount of plasmid DNA was kept constant (1 μg) with the empty plasmid. At 24 h after transfection, cells were selected with G418 (400 μg/ml) for 2 weeks. G418-resistant colonies were fixed in methanol, and stained with Giemsa's solution.

Abbreviations

CHX, cycloheximide; MEF, mouse embryonic fibroblasts; NF-κB, nuclear factor kappa B; TNF-α, tumor necrosis factor α; Ub, ubiquitin.

Acknowledgements

We thank members of our laboratory for helpful discussions. We also thank Y Nakamura for excellent technical assistance. We give special thanks to Dr M Karin for providing us with $p65^{-/-}$ MEF. This work was supported in part by a Grant-in-Aid from the Ministry of Health, Labour and Welfare for Third Term Comprehensive Control Research for Cancer, a Grant-in-Aid for Scientific Research on Priority Areas from the Ministry of Education, Culture, Sports, Science and Technology, Japan, and a Grant-in-Aid for Scientific Research from Japan Society for the Promotion of Science.

References

Agami R, Blandino G, Oren M, Shaul Y. (1999). *Nature* **399**: 809–813.
Balint E, Bates S, Vousden KH. (1999). *Oncogene* **18**: 3923–3929.
Bayon Y, Ortiz MA, Lopez-hernandez FJ, Gao F, Karin M, Pfahl M *et al.* (2003). *Mol Cell Biol* **23**: 1061–1074.
Beg AA, Baltimore D. (1996). *Science* **274**: 782–784.
Beg AA, Sha WC, Bronson RT, Baltimore D. (1995). *Nature* **376**: 167–170.
Bernassola F, Salomoni P, Oberst A, Di Como CJ, Pagano M, Melino G *et al.* (2004). *J Exp Med* **199**: 1545–1557.
Bourdon JC, Fernandes K, Murray-Zmijewski F, Liu G, Diot A, Xirodimas DP *et al.* (2005). *Genes Dev* **19**: 2122–2137.
Chang L, Kamata H, Solinas G, Luo JL, Maeda S, Venuprasad K *et al.* (2006). *Cell* **124**: 601–613.
Flores ER, Tsai KY, Crowley D, Sengupta S, Yang A, McKeon F *et al.* (2002). *Nature* **416**: 560–564.
Fontemaggi G, Gurtner A, Strano S, Higashi Y, Sacchi A, Piaggio G *et al.* (2001). *Mol Cell Biol* **21**: 8461–8470.
Gong J, Costanzo A, Yang HQ, Melino G, Kaelin Jr WG, Levrero M *et al.* (1999). *Nature* **399**: 806–809.
Gressner O, Schilling T, Lorenz K, Schulze Schleithoff E, Koch A, Schulze-Bergkamen H *et al.* (2005). *EMBO J* **24**: 2458–2471.
Grob TJ, Novak U, Maisse C, Barcaroli D, Luthi AU, Pirnia F *et al.* (2001). *Cell Death Differ* **8**: 1213–1223.
Huang TT, Wuerzberger-Davis SM, Seufzer BJ, Shumway SD, Kurama T, Boothman DA *et al.* (2000). *J Biol Chem* **275**: 9501–9509.
Ikawa S, Nakagawara A, Ikawa Y. (1999). *Cell Death Differ* **6**: 1154–1161.
Irwin MS, Kondo K, Marin MC, Cheng LS, Hahn WC, Kaelin Jr WG. (2003). *Cancer Cell* **3**: 403–410.
Jost CA, Marin MC, Kaelin Jr WG. (1997). *Nature* **389**: 191–194.
Kaghad M, Bonnet H, Yang A, Creancier L, Biscan JC, Valent A *et al.* (1997). *Cell* **90**: 809–819.
Kawai H, Nie L, Yuan ZM. (2002). *Mol Cell Biol* **22**: 6079–6088.
Kharbanda S, Ren R, Pandey P, Shafman TD, Feller SM, Weichselbaum RR *et al.* (1995). *Nature* **376**: 785–788.
Kim JS, Lee JM, Chwae YJ, Kim YH, Lee JH, Kim K *et al.* (2004). *Biochem Pharmacol* **67**: 1459–1468.
Kramer S, Ozaki T, Miyazaki K, Kato C, Hanamoto T, Nakagawara A. (2005). *Oncogene* **24**: 938–944.
Lee CW, La Thangue NB. (1999). *Oncogene* **18**: 4171–4181.
Leng RP, Lin Y, Ma W, Wu H, Lemmers B, Chung S *et al.* (2003). *Cell* **112**: 779–791.
Lissy NA, Davis PK, Irwin M, Kaelin Jr WG, Dowdy SF. (2000). *Nature* **407**: 642–645.
Mantovani F, Piazza S, Gostissa M, Strano S, Zacchi P, Mantovani R *et al.* (2004). *Mol Cell* **14**: 625–636.
Melino G, De Laurenzi V, Vousden KH. (2002). *Nat Rev Cancer* **2**: 605–615.
Muta T, Takeshige K. (2001). *Eur J Biochem* **268**: 4580–4589.
Nakagawa T, Takahashi M, Ozaki T, Watanabe K, Todo S, Mizuguchi H *et al.* (2002). *Mol Cell Biol* **22**: 2575–2585.
Pozniak CD, Radinovic S, Yang A, McKeon F, Kaplan DR, Miller FD. (2000). *Science* **289**: 304–306.
Rossi M, De Laurenzi V, Munarriz E, Green DR, Liu YC, Vousden KH *et al.* (2005). *EMBO J* **24**: 836–848.
Stiewe T, Putzer BM. (2002). *Cell Death Differ* **9**: 237–245.
Stiewe T, Zimmermann S, Frilling A, Esche H, Putzer BM. (2002). *Cancer Res* **62**: 3598–3602.
Strano S, Monti O, Pediconi N, Baccarini A, Fontemaggi G, Lapi E *et al.* (2005). *Mol Cell* **18**: 447–459.
Van Antwerp DJ, Martin SJ, Kafri T, Green DR, Verma IM. (1996). *Science* **274**: 787–789.
Wan YY, DeGregori J. (2003). *Immunity* **18**: 331–342.
Wang CY, Mayo MW, Baldwin ASJ. (1996). *Science* **274**: 784–787.
Wang CY, Mayo MW, Korneluk RG, Goeddel DV, Baldwin SJ. (1998). *Science* **281**: 1680–1683.
Yamagishi N, Miyakoshi J, Takebe H. (1997). *Int J Radiat Biol* **72**: 157–162.
Yang A, Kaghad M, Wang Y, Gillett E, Fleming MD, Dotsch V *et al.* (1998). *Mol Cell* **2**: 305–316.
Yang A, McKeon F. (2000). *Nat Rev Mol Cell Biol* **1**: 199–207.
Yang A, Walker N, Bronson R, Kaghad M, Oosterwegel M, Bonnin J *et al.* (2000). *Nature* **404**: 99–103.
Yuan ZM, Shioya H, Ishiko T, Sun X, Gu J, Huang YY *et al.* (1999). *Nature* **399**: 814–817.
Zaika AI, Slade N, Erster SH, Sansome C, Joseph TW, Pearl M *et al.* (2002). *J Exp Med* **196**: 765–780.
Zeng X, Chen L, Jost CA, Maya R, Keller D, Wang X *et al.* (1999). *Mol Cell Biol* **19**: 3257–3266.

Supplementary Information accompanies the paper on the Oncogene website (http://www.nature.com/onc).

Nanokinetics of drug molecule transport into a single cell

Atsushi Tamura[1], Koichiro Ozawa[1], Tatsuo Ohya[1], Naohiro Tsuyama[1], Edward M Eyring[2] & Tsutomu Masujima[1†]

†Author for correspondence
[1]Analytical Molecular Medicine and Devices Laboratory, Graduate School of Medical Sciences, Hiroshima University, 1-2-3 Kasumi, Minami-ku, Hiroshima 734-8551, Japan
Tel.: +81 82 257 5301; Fax: +81 82 257 5304; E-mail: tsutomu@hiroshima-u.ac.jp
[2]Department of Chemistry, University of Utah, Salt Lake City, UT 84112, USA

Aims: To analyze drug transport at a single cell level, a mast cell line, RBL-2H3, was treated with cell-permeable fluorescent compounds, such as quinacrine, and was monitored by a fluorescence video microscope. **Methods:** Small areas in the video that corresponded to granules and part of the cytosol in a cell were chosen and the signal intensity in these areas was monitored sequentially. **Results:** The initial rate of quinacrine uptake through the cell membrane calculated from the fluorescent signal was correlated with quinacrine concentration, and it decreased at a lower temperature, showing that the transport was an energy-requiring process, such as active transport. The kinetics of the transport through the microgranular membrane did not depend on the temperature but the pH in the cytosol, therefore this process should be passive transport by pH gradient. **Conclusion:** These data indicate that the observation of video microscope-mediated drug transport using fluorescent dye is useful in kinetic analysis at the nanometer scale.

Keywords: drug transport, image analysis, mast cell, nanokinetics, quinacrine, video microscope

The molecular dynamism in cells or tissues is one of the essential bases for nanomedicine; therefore, analytical methods should be developed to study it. The video microscopic method is useful not only for visualizing the cell morphologically [1–5], but also for analyzing molecular dynamism, such as molecular movement and content variations, using fluorescent probes or other probing techniques [6–9].

We have studied video microscopic imaging analysis, which provides morphological observations of object-oriented cellular responses, including molecular mechanisms [5,10,11]. This indicated that the signal intensity of a certain area in a video image could be used for quantitative analysis at a high magnification and even a single molecule can be seen as a faint dot [12,13].

The rat basophilic leukemia cell line, RBL-2H3, is used frequently as a model of mucosal mast cells [14,15] and has been studied widely to analyze the mechanism of the exocytotic process [16]. The cells have many acidic microgranules, which stably contain basic neurotransmitters, such as histamine and serotonin. We found that these granules stained easily with a cell-permeable fluorescent compound, quinacrine (QC), which is a weakly basic molecule. As acidic granules can be stained with QC, this compound was used as an indicator for cellular pH [17]. In addition, a QC derivative was used formerly as an antimalarial drug and is now used as an inhibitor of phospholipase A_2 in cell biology experiments [18].

In this report, we applied the video microscopic method to analyze the dynamics of drug transport into a single cell and further to submicrometer size (0.2–0.8 µm diameter) acidic granules in which drug molecules are specifically concentrated. This kinetic analysis at the nanometer scale is called 'nanokinetics' [19] and we think that an understanding of nanokineticis is important for nanomedicine.

Materials & methods

Cell culture

The rat basophilic leukemia cell line, RBL-2H3, was cultured in minimal essential medium (Invitrogen, Carlsbad, CA, USA) supplemented with 15% fetal bovine serum (Irvine Scientific, Santa Ana, CA, USA), penicillin G (100 U/ml; Invitrogen) and streptomycin (100 µg/ml; Invitrogen) in a humidified incubator with 5% CO_2 and 95% air at 37°C. The day before the experiment, cells were inoculated onto glass cover slips at 5×10^4 cells/cm^2, as described previously [10].

Fluorescent microscopic observation

An inverse-type incident-light fluorescence microscope (Axiovert 135-TV; Carl Zeiss Oberkochen, Germany) with a differential interference contrast (DIC) illumination system

10.2217/17435889.1.3.345 ISSN 1743-5889

Figure 1. Scheme of quinacrine uptake analysis.

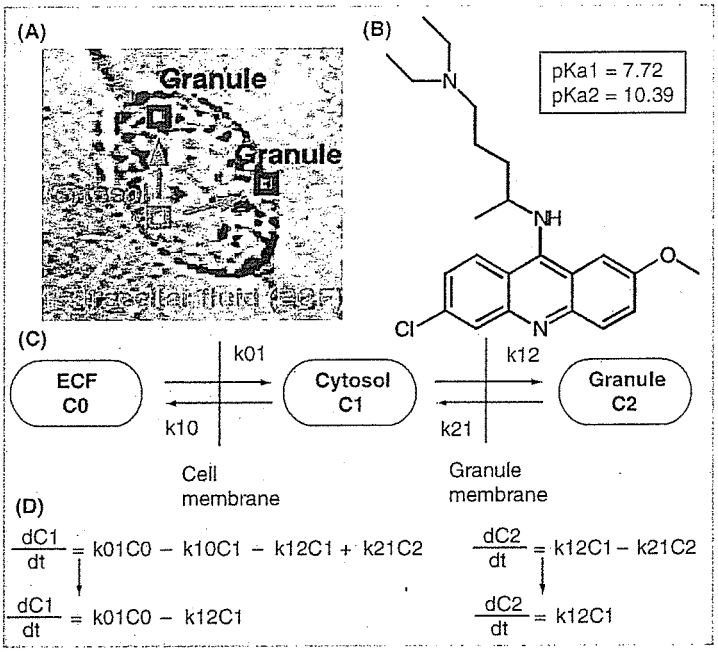

(A) DIC image of a RBL-2H3 cell. The areas of fluorescent signal analysis were selected as indicated. **(B)** The molecular formula and pKa [21] of QC is indicated. **(C)** QC transport was analyzed using the two-compartmental model. **(D)** The formula of the model was converted as described.
DIC: Differential interference contrast; QC: Quinacrine.

and silicon-intensified target (SIT) video camera (C-2741; Hamamatsu Photonics, Hamamatsu, Japan) was used for fluorescence video imaging. The whole microscopic system was placed in a temperature-controlled room. The image was recorded by a video tape recorder and analyzed by graphic analysis system (GBP-1, Sharp Semiconductor, Tokyo, Japan) installed on a personal computer. This system allows a sequential analysis of signal intensity in a certain area of a video picture, with optical resolution in the X–Y plane at 200 nm and focus depth (Z-axis) of 400 nm, by using an objective lens for 100-times magnification. Using image procesing methods, such as the video-enhancement contrast method, the image can be modified to provide a more resolved image, however, we cannot overcome the theoretical optical wavelength limitation in the resolution. To obtain reproducible data without compensation, we always used the same system conditions, such as experimental temperature, SIT camera control, including gain and amplification value, and neutral density filters. After obtaining the video image, small areas (9 × 9 pixels square each) corresponding to microgranules or part of the cytosol were chosen and the value of the fluorescent intensity was obtained sequentially and used for further analysis.

Quantification of QC

In order to analyze the QC concentration in the cells, a standard curve of QC concentration and fluorescence intensity was constructed by measuring the fluorescence of QC solutions (0.001, 0.01, 0.1, 1 and 10 µmol/l) in culture dishes using the video microscope, as described above. Since the fluorescence intensity of a QC solution changes according to the pH, we analyzed the relevance of the fluorescence of QC to pH. The fluorescence of the QC solution adjusted to various pH by Briotn-Robinson wide-range buffer was measured by a fluorecence spectrometer and the correlation coefficient was calculated using a pH–fluorescence correlation curve.

Compartmental analysis

Two-compartmental analysis was used for this QC transport system as shown in Figure 1. Equation 1 represents the transport across the cell membrane between extracellular medium and cytoplasm, where C0, C1 and C2 are the concentration of QC in medium, cytoplasm and a granule, respectively, and k01, k10, k12 and k21 are the transport kinetic constants of uptake from the medium to the cytosol, feedback from the cytosol to medium, uptake from the cytosol to a granule and feedback from a granule to the cytosol, respectively.

Equation 1:

$$dC1/dt = k01C0 - k10C1 - k12C1 + k12C2$$

Equation 2 represents the transport between cytoplasm and granules across the granular membrane:

$$dC2/dt = k12C1 - k21C2$$

The concentration of QC was measured by the fluorescence intensity in the video image. We measured the starting increasing rate, so the inverse reaction can be neglected. Therefore, these equations are changed to:

Equation 3:

$$dC1/dt = k01C0 - k12C1$$

Equation 4:

$$dC2/dt = k12C1$$

Since dC1/dt, dC2/dt and C1 are measured by video signal intensity analysis and C0 is known, k01 and k12 can be estimated.

Figure 2. 0.1 and 1 μM quinacrine uptake into RBL-2H3 cells.

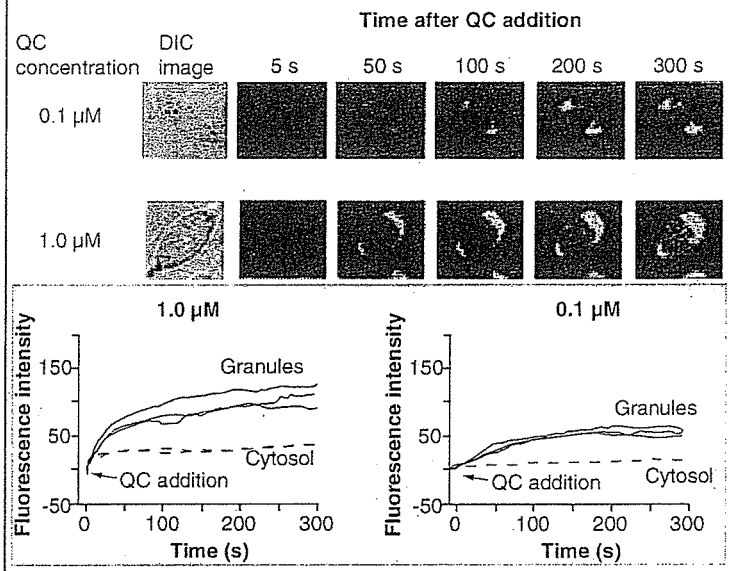

The upper pictures show DIC images of analyzed RBL-2H3 cells before QC addition and time-lapse fluorescent images after QC addition. Cytosolic and granular fluorescence increased gradually after QC addition. In the lower graphs, fluorescence intensity of selected areas in the cytosol and microgranules (three areas each) after QC addition was plotted. The arrows show the time of QC addition. Data are representative of three independent experiments.
DIC: Differential interference contrast; QC: Quinacrine.

Results & discussion

Figures 2 & 3 (upper columns) show QC transport into RBL-2H3 cells in a DIC image and time-lapse fluorescence images. The fluorescence intensity was estimated by the video image intensity in each area (in the cytosol and granules), as described above. After adding QC to the culture buffer, the fluorescence intensities were monitored according to time. At lower concentration, QC transported into the cells rather slowly through the cell membrane; however, above 1.0 μm of QC, the rate of transport had almost started to maximize and the intensity of fluorescence of QC became saturated within 1 min (Figure 2 and data not shown). The estimated uptake rates of QC by fluorescence intensity at the early step (0–15 s; n = 3) are summarized in Table 1. The rate of increasing fluorescence was concentration dependent both in the cytosol and in granules. With these rates, and Equations 3 & 4, k01 and k12 were evaluated as in Table 1. The value of k01 decreased according to the increase in the outside concentration of QC. The transportation was not speedy enough even when the medium concentration was high. By contrast, the inner transport from cytosol to microgranules was almost constant and not dependent on the concentration of medium QC.

In order to investigate the requirement of energy for is transport, the same analysis was performed at two different temperatures (24 and 14°C), as shown in Figure 3. The initial rates of QC transport measured by the fluorescence at two different temperatures were decreased drastically to 1/20 and 1/10 for cytosol and granules by the decrease in temperature of 10°C (Table 2). However, only the rate constant of the first transport step (k01: from medium to cytosol) decreased ten-times, with k12 remaining unchanged. This showed that transport through the cell membrane was an energy-requiring process, such as active transport, but the second step was not energy dependent and is an autodiffusion process.

Since the interiors of the microgranules of this mast cell type are known to be acidic [20], the weakly basic molecule, QC [21], appeared to be transported by the pH gradient between the cytosol and granules. In order to reduce this pH

Table 1. The kinetics of quinacrine uptake at various quinacrine concentrations.

The initial rate of QC uptake

Quinacrine (μM)	*Cytoplasm (SD)*	*Granules (SD)*
0.001	0.057 (0.006)	0.13 (0.01)
0.01	0.16 (0.02)	0.28 (0.03)
0.1	0.85 (0.08)	1.48 (0.13)
1	2.92 (0.08)	6.0 (0.8)
10	9.02 (0.09)	19.4 (0.2)
	(Fluorescence intensity/sec)	

The constant of QC uptake

Quinacrine (μM)	*K01*	*K12*
0.001	0.183	0.31
0.01	4.4×10^{-2}	0.44
0.1	2.3×10^{-2}	0.21
1	8.9×10^{-3}	0.25
10	2.8×10^{-3}	0.19
		(1/sec)

The rate of QC uptake was calculated from the initial slope (within 60 s). The data shown are the average of three independent experiments. The constants were calculated using the formula from **Figure 1**. *SD: Standard deviation of the values for initial rates of QC uptake.*

Figure 3. 0.1 μM quinacrine uptake into RBL-2H3 cells at 24 and 14°C.

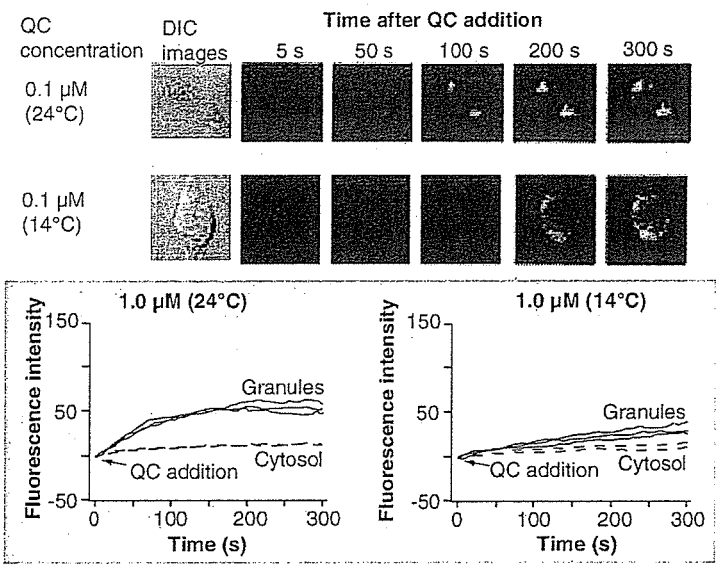

QC uptake was compared between the culture temperature, 24 and 14°C. The upper pictures show DIC images of RBL-2H3 cells before QC addition and time-lapse fluorescent images after QC addition. Cytosolic and granular fluorescence increased gradually after QC addition. In the lower graphs, fluorescence intensity of relevant areas to cytosol and microgranules (three areas each) after QC addition was plotted. The arrows show the time of QC addition. Data are representative of three independent experiments.
DIC: Differential interference contrast; QC: Quinacrine.

gradient, ammonium chloride was introduced to the medium to neutralilze the acidic environment of the microgranule, as seen in Figure 4 (upper panel). The transport into the cytosol was stimulated, judging from the starting rate, as shown in Figure 4 (lower right); however, k01 showed a small increase and k12, transport through the microgranule membrane, decreased by half. This shows that the transport into the microgranule seems to be pH dependent.

In this analysis, we have not measured the intracellular pH exactly, but have used the reported pH value of the cytosol and microgranules [20]. In addition, we compensated the fluorescence value simply by pH, but it is possible that another factor, such as oxidation or degradation of QC, might affect the fluorescence. The further analysis of QC molecules using mass spectrometry might provide the information on QC status inside the cytosol and microgranules.

Conclusions

The dynamic aspect of drug transport in the cytosol and microgranules in a single cell was analyzed to quantitate its 'nanokinetics' by using a 2D video detector. It was found that the quinacrine uptake through this RBL-2H3 cell membrane is an energy-requiring process, such as active transport. However, the transport through the microgranular membrane depended on the pH in the cytosol, as opposed to the temperature, as with passive transport by a pH gradient. The video microscopic method of visualizing drug transport in a cell is useful in kinetic analysis at the nanoscale.

Future perspective

When observing the behavior of nanoparticles in solutions at the submicron scale, movements of the nanoparticles are very dynamic. Nanoparticles move rapidly and are randomly driven by Brownian motion. Such a dynamic image of molecular movement could be produced in any nanoscale biosystem and showed an approach towards the quantitative estimation of the nanodynamics of molecules in a single cell. The nanokinetic understanding of medicinal molecules inside cells or in tissues, even in microorgans, will help the development of future nanomedicine applications, especially for more dynamic applications.

Acknowledgements

This research was supported partly by the Japan Ministry of Education, Science, Sports and Culture, Grant-in-Aid for Scientific Research.

Table 2. The kinetics of quinacrine uptake at various temperatures.

The initial rate of QC uptake

Temperature (°C)	*Cytoplasm (SD)*	*Granules (SD)*
24	0.85 (0.12)	1.5 (0.1)
14	0.043 (0.002)	0.14 (0.02)
	(Fluorescence intensity/sec)	

The constant of QC uptake

Temperature (°C)	*K01*	*K12*
24	2.2×10^{-2}	0.21
14	1.8×10^{-3}	0.16
		(1/sec)

The rate of QC uptake was calculated from the initial slope (within 60 s). The data shown are the average of three independent experiments. The constants were calculated using the formula from **Figure 1**.
SD: Standard deviation of the values for initial rates of QC uptake.

Figure 4. 1 μM quinacrine uptake into RBL-2H3 cells with or without 10 mm ammonium chloride.

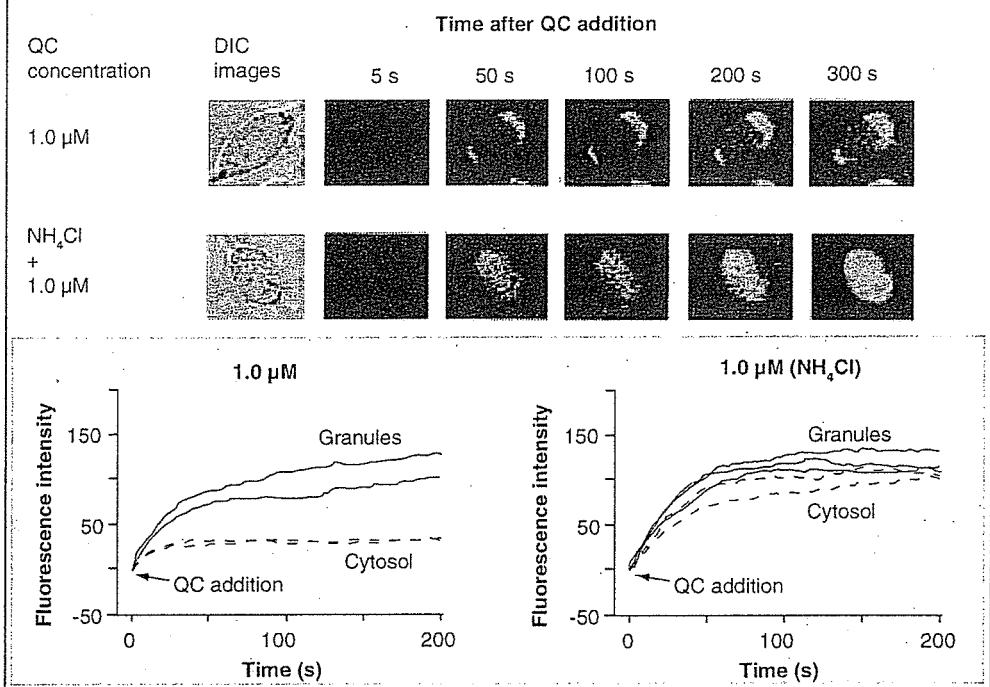

QC uptake was compared with and without 10 mM NH_4Cl (pH 7.4 vs pH 5.6, respectively). The upper pictures show DIC images of RBL-2H3 cells before QC addition and time-lapse fluorescent images after QC addition. Cytosolic and granular fluorescence increased gradually after QC addition. In the lower graphs, fluorescence intensity of relevant areas to cytosol and microgranules (three areas each) after QC addition was plotted. The arrows show the time of QC addition. Data were representative of three independent experiments.
DIC: Differential interference contrast; QC: Quinacrine.

Executive summary

Nanokinetics: subcellular kinetics in a single cell

- Subcellular molecular dynamism, such as drug transport through a cell membrane and micro-organ membrane in a single cell should be clarified for future nanomedicine design.

Video microscope as a tool for nanokinetic analysis

- Video microscopic imaging of a fluorescent drug molecule, quinacrine, in a single cell of mast cell model, RBL-2H3, was performed.
- 2D light-intensity data of video images were useful for nanokinetic analysis.

Results of nanokinetic analysis

- Quinacrine uptake through the RBL-2H3 cell membrane is an energy-requiring process, such as active transport.
- Transport through the microgranular membrane did not depend on the temperature but on the pH in the cytosol, such as passive transport by pH gradient.

Future perspetive

- Nanokinetic understanding of molelcular transport will be the basis for future designing in nanomedicine, such as micro-shot drug delivery and micro-organ-targeted treatment.

Bibliography

1. Martin PM, Magdelenat HP, Benyahia B, Rigaud, O, Katzenellenbogen JA: New approach for visualizing estrogen receptors in target cells using inherently fluorescent ligands and image intensification. *Cancer Res.* 43(10), 4956–4965 (1983).
2. Wadsworth P, Sloboda RD: Microinjection of fluorescent tubulin into dividing sea urchin cells. *J. Cell Biol.* 97(4), 1249–1254 (1983).
3. Weiss D, Galfe G: Video-microscopic techniques to study the living cytoplasm. In: *Image Analysis in Biology.* Hader DP (Ed.). CRC Press, Boca Raton, USA, 135–158 (1992).
4. Terakawa S, Suzuki Y: Exocytosis in colonic goblet cells visualized by video-enhanced light microscopy. *Biochem. Biophys. Res. Commun.* 176(1), 466–472 (1991).
5. Suzaki E, Kobayashi H, Kodama Y, Masujima T, Terakawa S: Video-ratedynamics of exocytotic events

associated with phagocytosis in neutrophils. *Cell Motil. Cytoskeleton* 38(3), 215–228 (1997).

6. Saengkhae C, Loetchutinat C, Garnier-Suillerot A: Kinetic analysis of fluorescein and dihydrofluorescein effluxes in tumour cells expressing the multidrug resistance protein, MRP1. *Biochem. Pharmacol.* 65(6), 969–977 (2003).

7. Csala M, Staines AG, Banhegyi G *et al.*: Evidence for multiple glucuronide transporters in rat liver microsomes. *Biochem. Pharmacol.* 68(7), 1353–1362 (2004).

8. Schwartz JW, Novarino G, Piston DW, DeFelice LJ: Substrate binding stoichiometry and kinetics of the norepinephrine transporter. *J. Biol. Chem.* 280(19), 19177–19184 (2005).

9. Petrasek J, Mravec J, Bouchard R *et al.*: PIN proteins perform a rate-limiting function in cellular auxin efflux. *Science* 312, 914–918 (2006).

10. Ozawa K, Kobayashi H, Kawai E, Suzaki E, Nonomura Y, Masujima T: Quantitative analysis of exocytosis visualized by a video-enhanced light/fluorescence microscope reveals two distinct components of exocytosis in RBL-2H3 cells. *FEBS Lett.* 398(1), 67–73 (1996).

11. Ozawa K, Masujima T, Ikeda K, Kodama Y, Nonomura Y: Different pathways of inhibitory effects of wortmannin on exocytosis are revealed by video-enhanced light microscope. *Biochem. Biophys. Res. Commun.* 222(2), 243–248 (1996).

12. Funatsu T, Harada Y, Tokunaga M, Saito K, Yanagida T: Imaging of single fluorescent molecules and individual ATP turnovers by single myosin molecules in aqueous solution. *Nature* 374(6522), 555–559 (1995).

13. Harada Y, Funatsu T, Murakami K, Nonoyama Y, Ishihama A, Yanagida T: Single-molecule imaging of RNA polymerase-DNA interactions in real time. *Biophys. J.* 76(2), 709–715 (1999).

14. Beaven MA, Maeyama K, Wolde-Mussie E, Lo TN, Ali H, Cunha-Melo JR: Mechanism of signal transduction in mast cells and basophils: studies with RBL-2H3 cells. *Agents Actions* 20(3–4), 137–145 (1987).

15. Seldin DC, Adelman S, Austen KF *et al.*: Homology of the rat basophilic leukemia cell and the rat mucosal mast cell. *Proc. Natl Acad. Sci. USA* 82(11), 3871–3875(1985).

16. Kawasaki Y, Saitoh T, Okabe T, Kumakura K, Ohara-Imaizumi M: Visualization of exocytotic secretory processes of mast cells by fluorescence techniques. *Biochim. Biophys. Acta* 1067(1), 71–80 (1991).

17. Korf BR, Schuh BE, Salwen MJ: Optimum pH for nuclear sex identification using quinacrine. *Clin. Genet.* 8(2), 145–148 (1975).

18. Nakadate T, Yamamoto S, Ishii M, Kato R: Inhibition of 12-*O*-tetradecanoylphorbol-13-acetate-induced epidermal ornithine decarboxylase activity by lipoxygenase inhibitors: possible role of product(s) of lipoxygenase pathway. *Carcinogenesis* 3(12), 1411–1414 (1982).

19. Suzuto M, Hirakawa Y, Ohnishi H *et al.*: Nano-kinetics of probe-particles in solution visualized by a pin-fiber video scope. *Anal. Sci.* 19(1), 43–47 (2003).

20. Sussman Y, Reck B, Pecht I: Mutual relationship among cytosolic pH, Na^+ and Ca^{2+} ions in the degranulation of rat leukemic basophils. *Immunol. Lett.* 13(4), 215–219 (1986).

21. Liao X, Wiedmann TS: Solubilization of cationic drugs in lung surfactant. *Pharm. Res.* 20(11), 1858–1863 (2003).

Chemosensitivity prediction in esophageal squamous cell carcinoma: Novel marker genes and efficacy-prediction formulae using their expression data

TATSUSHI SHIMOKUNI[1,7], KEIJI TANIMOTO[1], KEIKO HIYAMA[1], KEIKO OTANI[2], MEGU OHTAKI[2], JUN HIHARA[3], KAZUHIRO YOSHIDA[3], TSUYOSHI NOGUCHI[4], KATSUNOBU KAWAHARA[4], SHOJI NATSUGOE[5], TAKASHI AIKOU[5], YASUSHI OKAZAKI[6], YOSHIHIDE HAYASHIZAKI[6], YUJI SATO[7], SATORU TODO[7], EISO HIYAMA[8] and MASAHIKO NISHIYAMA[1]

Departments of [1]Translational Cancer Research, [2]Environmetrics and Biometrics, and [3]Surgical Oncology, Research Institute for Radiation Biology and Medicine, Hiroshima University, Hiroshima 734-8553; [4]Department of Surgery II, Faculty of Medicine, Oita University, Oita 879-5593; [5]Department of Surgical Oncology, Digestive Surgery, Graduate School of Medicine, Kagoshima University, Kagoshima 890-8544; [6]Laboratory for Genome Exploration Research Group, Riken Genome Science Center, Riken Yokohama Institute, Yokohama 230-0045; [7]Department of General Surgery, Graduate School of Medicine, Hokkaido University, Sapporo 060-8638; [8]Natural Science Center for Basic Research and Development, Hiroshima University, Hiroshima 734-8551, Japan

Received December 9, 2005; Accepted January 30, 2006

Abstract. Esophageal cancer is a highly lethal disease and the optimal therapy remains unclear. Since adjuvant chemotherapy gives a better chance of survival, we attempted to develop a chemosensitivity prediction model to improve individual responses to therapy. Comprehensive gene expression analyses (cDNA and oligonucleotide microarrays) and MTT assay of 8 drugs in 20 KYSE squamous cell carcinoma cell lines were performed to distinguish candidate marker genes whose expression levels reproducibly correlated with cellular drug sensitivities. After confirmation with real-time RT-PCR, we performed multiple regression analyses to develop drug-sensitivity prediction formulae using the quantified expression data of selected marker genes. Using the same sets of genes, we also constructed prediction models for individual clinical responses to 5-FU-based chemotherapy using 18 cases. We selected 5 better marker genes, known as drug sensitivity determinants, identified 9 novel predictive genes for 4 of 8 anti-cancer drugs [5-FU, CDDP, DOX, and CPT-11 (SN-38)], and developed highly predictive formulae of *in vitro* sensitivities to the 4 drugs and clinical responses to 5-FU-based adjuvant chemotherapies in terms of overall and disease-free survivals. Our selected genes are likely to be effective drug-sensitivity markers and formulae using the 9 novel genes would provide advantages in prediction.

Correspondence to: Dr Masahiko Nishiyama, Department of Translational Cancer Research, Research Institute for Radiation Biology and Medicine, Hiroshima University, 1-2-3 Kasumi, Minami-ku, Hiroshima 734-8553, Japan
E-mail: yamacho@hiroshima-u.ac.jp

Key words: personalized medicine, drug sensitivity, gene expression, esophageal cancer, microarray

Introduction

Esophageal squamous cell carcinoma (ESCC) is rarely curable and only occasionally, if the patient is diagnosed very early, is there a chance of survival (1). Patients usually have rapid tumor recurrence and distant metastasis, even after curative surgery. A variety of treatments, such as chemotherapy, radiation, and their combinations, have been intensively investigated to date, and adjuvant (or neoadjuvant) chemotherapy for ESCC patients is now considered to be one of the most potent methods for lengthening survival times (2-4). However, the therapeutic outcome significantly varies, even among patients given the same therapy. The prediction of sensitivity to anticancer drugs and clinical outcomes of chemotherapy, which would allow selection of an optimal regimen for each individual, is urgently required to improve survival rates for ESCC patients.

The importance of prior laboratory prediction of individual drug response has stimulated research to identify the most reliable biomarkers, and several molecular markers and gene expression profiles in tumor tissues have shown potential for predictive benefit (5-8). None of these markers, however, is consistently critical in drug response for ESCC. Despite DNA chip technology, which enables us to overview a huge number of gene expressions simultaneously, the approach to predicting individual drug response by expression pattern, 'the snapshot profile', is increasingly recognized as being limited (9,10). Drug sensitivity is determined by multiple genes, and gene expression

profiles in response to drug exposure vary considerably among individuals even for the same drug or regimen. The ingenious and intricate mechanisms of drug sensitivity create obstacles to predicting the therapeutic efficacy of a drug, so a concise laboratory prediction system which can overcome the obstacles is eagerly awaited.

We have attempted to develop such a prediction system, and have shown the first concise prediction models of the *in vitro* activity for 8 drugs (5-FU, CDDP, MMC, DOX, CPT-11, SN-38, TXL, and TXT) using 19 cancer cell lines of various origin, along with individual clinical responses to 5-FU using the expression data of 12 genes selected solely from 50 function-proven genes (11). In that study, we used only cDNA microarray to distinguish potential prediction marker genes, followed by confirmation analysis with real-time RT-PCR. Consequently, there was no effective way to determine critical marker genes from the huge number of candidates, and we selected only functionally proven genes. However, it is obvious that more important marker genes may exist among the huge number of functionally unknown genes. Moreover, the biological behavior and molecular basis of cancer differ significantly according to its origin, so more prominent prediction biomarkers of drug response specific to each type of cancer may exist. Thus, we focused on ESCC and used oligonucleotide microarray analyses together with cDNA microarray to select more powerful drug-sensitivity markers. Using selected genes with and without proven functional significance to drug sensitivity, we developed an *in vitro* prediction model in 20 ESCC cell lines and then constructed a clinical application model, a prediction system of therapeutic response to 5-fluorouracil (5-FU) based chemotherapy.

Materials and methods

Chemicals. 5-FU, Mitomycin C (MMC), and Doxorubicin (DOX) were kindly provided by Kyowa Hakko Kogyo Co., Ltd. (Tokyo, Japan). Cisplatinum (CDDP) and paclitaxel (TXL) were generously provided by Bristol-Myers K. K. (Tokyo, Japan). Docetaxel (TXT) was purchased from Aventis Pharma Ltd. (Tokyo, Japan), and irinotecan (CPT-11) and its active metabolite, SN-38, were obtained from Yakult Honsha Co., Ltd. (Tokyo, Japan). All other chemicals were of analytical grade and were purchased from Wako Pure Chemicals (Osaka, Japan) and Sigma (St. Louis, MO, USA).

Cells. A total of 21 cell strains/lines, 1 non-cancerous esophageal epithelial cell strain (HEEC-1) and 20 KYSE human esophageal squamous cell carcinoma cell lines (KYSE-30, -140, -150, -170, -180, -200, -220, -350, -410, -450, -510, -520, -590, -770, -850, -890, -1170, -1190, -1250, and -2270) were kindly provided by Dr Y. Shimada (Kyoto University, Kyoto, Japan). Human cancer cell lines were cultured in RPMI-1640 medium (Life Technologies, Inc., Grand Island, NY) containing 10% heat-inactivated fetal bovine serum (FBS; BioWhittaker, Verviers, Belgium) at 37°C in a humidified atmosphere of 5% CO_2 and maintained in continuous exponential growth by passage every 3 days. Non-cancerous HEEC-1 cells were cultured in Keratinocyte SFM medium with growth supplement containing 2.5 mg EGF and 25 mg bovine pituitary extract in 500 ml liquid basal medium (Gibco BRL, Rockville, MD) and expanded by passage twice in a week.

Patients and human tissue samples. Chemo-naïve patients with advanced esophageal cancer of which specimens could be collected at surgery were enrolled in the clinical study. All of the patients had histologically proven esophageal cancer (TNM/UICC classification: Stage III or IV) and had received curative esophagectomy with the subsequent 5-FU-based therapy as the post-operative adjuvant chemotherapy. The patients were all less than 80 years old (median 61, range 49-78) with performance status (World Health Organization: WHO) 0-2 without significant baseline-laboratory abnormalities, and life expectancy was estimated at more than 3 months. 5-FU was given by continuous intravenous administration at a dose of 250 mg/m^2 for 28 days or 5-day continuous-infusion of 500 mg/body/day per week for 28 days, as a combination regimen with cisplatin at an extremely low dose of 3 mg/m^2 or 10 mg/body/day. Total administered doses of 5-FU and CDDP ranged from 2,625 to 10,500 mg (median, 10,000 mg; mean, 8,912 mg), and 26 to 200 mg (median, 200 mg; mean, 143 mg), respectively. CT (computed tomography) scanning was performed every one or two months to evaluate disease-free survival (DFS). Overall survival (OS) was also estimated as the clinical response. Among the 18 tumor samples obtained from 17 patients, 14 tumors obtained early were used to yield the prediction formulae and 4 subsequently obtained tumors were used as test samples. Written informed consent was obtained from all patients, and the protocol was approved by our institutional ethics committees. The collected tumor specimens were stored at -80°C until use.

Extraction and purification of RNA. For gene expression analysis, exponentially growing cultured cells (2x10^6) were collected after two-washings with PBS. The cell pellets were immediately frozen in liquid nitrogen, and stored at -80°C until use. Cell pellets or frozen tissue samples (~40 mg) were powdered in liquid nitrogen, and total RNA was prepared using Qiagen RNeasy mini kit (Qiagen, Inc., Valencia, CA). For cDNA (complementary DNA) microarray analysis, mRNA was purified using μMACS mRNA Isolation kit (Miltenyi Biotec, Bergisch Gladbach, Germany) according to the supplier's protocols. The quality of the RNA was checked using Agilent Technologies 2100 Bioanalyzer (Agilent, Palo Alto, CA).

cDNA microarray analysis. RIKEN human 21K array containing 20,784 clones with positive and negative controls was used to analyze gene expression profiles of 20 KYSE esophageal cancer cell lines using HEEC-1 as a reference sample. The target DNA used to construct human 21 K array was the glycerol stock of cDNA clones purchased from ResGen (Invitrogen Corp., Carlsbad, CA). Fabrication of the microarray, hybridization, washing, and detection of signal intensities were described previously (12,13). Poly(A) RNAs from reference (HEEC-1) and sample (KYSE) cell lines were labeled, respectively, with Cy5-dCTP and Cy3-dCTP, by random-primed reverse transcription. Arrays were laser-scanned using ScanArray 5000™ confocal laser scanner (GSI Lumonics, Billerica, MA), and the images were analyzed using ScanAlyze™ (Stanford University). All experiments were

performed in duplicate. The amounts of mRNA were determined using the procedure proposed by Ohtaki *et al*, in which the signals of Cy3 and Cy5 were estimated as the value of ($\log_2 s$ - $\log_2 b$), where s is spot mean intensity and b is background median intensity. The signals were normalized by the procedure developed by Ohtaki *et al* and the normalized value was further standardized (14). The standardized value was obtained as follows and used as the amount of mRNA: $s^{Cy3**} = (u_i^* + v_i^*)/2$ and $s^{Cy5**} = (u_i^* - v_i^*)/2$, where u_i^*, and v_i^* are defined as u_i/h, and $[v_i - Q_{50}(v_i)]/h$, respectively. In the formulae, u_i and v_i represent the value of ($s^{Cy3*} + s^{Cy5*}$) and ($s^{Cy3*} - s^{Cy5*}$), while $Q_{75}(v_i)$, $Q_{50}(v_i)$, and $Q_{25}(v_i)$ indicate 75%, 50%, and 25% point of $\{v_i \mid i=1...21168\}$. s^{Cy3*} and s^{Cy5*} indicate normalized values of Cy3 and Cy5, and h indicates the half-hinge value, which is $h=(Q_{75}(v_i) - Q_{25}(v_i))/2$.

Oligonucleotide array analysis. Codelink Expression Bioarray System (Amersham Bioscience, Tokyo, Japan) was used according to the manufacturer's protocol. Briefly, first-strand cDNA was generated from 1 μg of total RNA of cell lines using reverse transcriptase and a T7 primer, and then second-strand cDNA was produced using DNA polymerase mix and RNase H. cRNA (complementary RNA) was generated via an *in vitro* transcription reaction using T7 RNA polymerase and biotin-11-UTP (Perkin-Elmer, Boston, MA), which was quantified by spectrometry and checked using Agilent 2100 Bioanalyzer™ (Agilent Technologies, Palo Alto, CA). Ten-micrograms of cRNA was then fragmented and hybridized to a Codelink™ Uniset Human 20K I Bioarray containing 19,981 probes with positive and negative bacterial control probes. After hybridization, the arrays were rinsed and labeled with Streptavidin-Cy5, scanned using Agilent DNA Microarray Scanner (Agilent), and then analyzed with Codelink Expression Analysis Software. Expression levels were normalized to the median expression value of the entire spot array. The microarray data were registered to the Gene Expression Omnibus under GE accession nos. GSE 2454 and GSE 2447 (http://www.ncbi.nlm.nih.gov.geo/).

Real-time RT-PCR (reverse transcription-polymerase chain reaction). Two-micrograms of total RNA extracted from each cell line or tissue was reverse-transcribed using a High-Capacity cDNA Archive™ kit (Applied Biosystems), and then 1,000 x aliquot of the cDNA (equivalent to 2 ng total RNA) from cell lines and 200 x aliquot of the cDNA (10 ng total RNA) from tissue were subjected to real-time RT-PCR using an ABI PRISM™ 7900HT sequence detection system (Applied Biosystems). Each reaction was carried out in triplicate or duplicate for cell lines and tissue, respectively, and averaged. The relative gene expression levels were calculated as a ratio to *GAPD* (glyceraldehyde-3-phosphate dehydrogenase gene) expression level.

Cytotoxicity assay. Drug-induced cytotoxicity was evaluated by conventional MTT [3-(4,5-dimethylthiazol-2-yl)-2,5-diphenyltetrazonium bromide] dye reduction assay. Cells were seeded in 96-MicroWell Plates (NUNCLON, NUNC, Roskilde, Denmark) at a density of $4x10^3$/well in RPMI-1640 with 10% FBS (fetal bovine serum). After 24-h incubation, the medium was replaced and cells were exposed to the indicated drug concentrations for 72 h, after which 10 μl of 0.4% MTT reagent and 0.1 M sodium succinate were added to each well. After 2-h incubation, 150 μl of DMSO was added to dissolve the purple formazan precipitate. The formazan dye was measured spectrophotometrically (570-650 nm) using a MAXline™ microplate reader (Molecular Devices Corp., Sunnyvale, CA). The cytotoxic effect of each treatment was assessed by IC_{50} value (inhibitory drug concentration of 50% cell growth: drug concentration of 50% optical density of control).

Rank correlation coefficient. Using rank correlation coefficient, the Spearman's correlation coefficient between ranks of two sets of measurements, we evaluated the statistical significance with a p-value obtained from the Monte Carlo method by generating null distribution under the hypothesis that there was no correlation between any two sets of measurements.

Multiple regression analysis. The relationship between y (response variable) and x_{i1}, $x_{i2}...x_{ip}$ (explanatory variables) is formulated in the linear model, $y_i = \varepsilon+\theta_1 x_{i1} + \theta_2 x_{i2} +...+ \theta_p x_{ip}$, where ε is constant. Trimmed Least Squares Regression (TLSR) was performed to determine a set of effective genes that would satisfy the value of IC_{50}: ($\theta_1...\theta_p$) were estimated from the data ($x_{i1}...x_{ip}$) when we used gene expression levels and cellular sensitivity to drugs (IC_{50} value for each drug), respectively as the explanatory and the response variables. The TLSR is a robust regression method based on an extended algorithm of LMSR (Least Median Squares Regression) by Rousseeuw, which explores models using masked samples with large residuals (15). We used the software, NLReg, developed by Ohtaki (http://apollo.rbm.hiroshima-u.ac.jp/), which implemented the robust regression analysis. Outliers were identified by referring to the value of AIC (Akaike's information criterion) for each sample or checking residuals graphically, and a set of effective genes that satisfied the value of IC_{50} was explored.

Results

Screening of prediction marker genes by comprehensive gene expression analysis. Comprehensive gene expression analyses using cDNA and oligonucleotide microarrays and MTT assay were performed in 20 ESCC cell lines to distinguish genes which were correlative in expression level with the cytotoxicities of 8 drugs. The standardized expression level of each gene and IC_{50} value for each drug in 20 cell lines were ranked, and then we determined the correlation between ranks of the two sets of measurements to select correlative genes with drug sensitivity.

The rank correlation analyses demonstrated a large number of correlative genes in cDNA and oligonucleotide microarrays, respectively: 500 and 520 for 5-FU, 494 and 997 for MMC, 644 and 978 for DOX, 479 and 867 for CDDP, 437 and 1,105 for TXL, 416 and 291 for TXT, 619 and 311 for CPT-11, and 509 and 1,007 for SN-38 ($p<0.05$). From these, we selected reproducibly correlative genes with drug sensitivity by both microarray analyses as the first candidates for drug sensitivity

Table I. Predictive marker genes for drug-induced cytotoxicity.

A) Genes known as drug sensitivity determinants.

Gene		Correlation coefficient (R)				
		5-FU	DOX	CDDP	CPT-11	SN-38
BCL2	cDNA		-			
	Oligo		0.505[b]			
	PCR		0.423[b]			
DPYD	cDNA	-				
	Oligo	0.475[b]				
	PCR	0.682[b]				
GSTP1	cDNA			-0.525[b]		
	Oligo			-0.430[c]		
	PCR			-0.426[c]		
MGMT	cDNA					-
	Oligo					0.412[c]
	PCR					0.538[b]
XRCC1	cDNA				0.589[b]	0.459[b]
	Oligo				-	-
	PCR				0.525[b]	0.392[c]

B) The highest correlative genes for drug sensitivity.

Gene		Correlation coefficient (R)				
		5-FU	DOX	CDDP	CPT-11	SN-38
ARFRP1	cDNA			0.615[a]		
	Oligo			0.565[a]		
	PCR			0.440[c]		
B4GALT5	cDNA	0.632[a]				
	Oligo	0.662[a]				
	PCR	0.772[a]				
CALU	cDNA				0.577[a]	
	Oligo				0.577[a]	
	PCR				0.423[c]	
IFITM1	cDNA			-0.630[a]		
	Oligo			-0.734[a]		
	PCR			-0.567[a]		
KIAA0685	cDNA			-0.567[a]		
	Oligo			-0.570[a]		
	PCR			-0.462[b]		
NRCAM	cDNA		0.645[a]			
	Oligo		0.653[a]			
	PCR		0.493[b]			
SIPA1L2	cDNA			-0.737[a]		
	Oligo			-0.595[a]		
	PCR			-0.499[b]		
UGCG	cDNA	0.579[a]				
	Oligo	0.578[a]				
	PCR	0.656[a]				
XBP1	cDNA	0.776[a]				
	Oligo	0.569[a]				
	PCR	0.804[a]				

cDNA, cDNA microarray analysis; oligo, oligonucleotide array analysis; PCR, real-time RT-PCR (linear regression analysis); [a]$p<0.01$; [b]$0.01 \leq p<0.05$; [c]$0.05 \leq p<0.1$.

markers: The numbers were 30 for 5-FU, 43 for MMC, 78 for DOX, 38 for CDDP, 41 for TXL, 43 for TXT, 30 for CPT-11, and 56 for SN-38 ($p<0.05$).

Determination of prediction marker genes using real-time RT-PCR. The aim was to determine reliable prediction markers for 8 drugs from each of the 359 candidates. First, we focused on 50 genes whose functions as drug sensitivity factors had been clearly demonstrated in at least 2 reports among a total of 897 related papers (11), but the 359 candidates included very few genes known as drug sensitivity determinants. Although we extended the screening field to a range of $p<0.1$ in either cDNA or oligonucleotide microarray screening, no possible markers were found for TXL- and TXT-induced cytotoxicity, and the number of selected genes was only 11: *DPYD* (dihydropyrimidine dehydrogenase gene) and *UMPS* (uridine monophosphate synthetase gene) for 5-FU; *ABCB1* (ATP-binding cassette, sub-family B, member 1 gene) for MMC; *MYC* (v-myc avian myelocytomatosis viral oncogene homolog) and *BCL2* (B-cell CLL/lymphoma 2 gene) for DOX, *GSTP1* (glutathione S-transferase π1 gene) and *GCLC* (glutamate-cysteine ligase, catalytic subunit gene) for CDDP; *TOP1* (topo-isomerase I gene) and *XRCC1* (X-ray repair complementing defective repair in Chinese hamster cells 1 gene) for CPT-11; *MGMT* (O^6-methylguanine-DNA methyltransferase gene), and *POR* [P-450 (cytochrome) reductase gene], *TOP1*, and *XRCC1* for SN-38 (16-37). These selected candidates were subjected to real-time RT-PCR analysis and we confirmed only 5 correlations: *DPYD* with 5-FU, *BCL2* with DOX, *GSTP1* with CDDP, *XRCC1* with CPT-11, and *MGMT* with SN-38, even when the selection criterion was determined as $p<0.1$ in the linear regression analysis (Table IA).

The very small number of marker genes for limited drugs encouraged us to select additional potent marker genes via another approach, using only the data of expression-sensitivity correlation analysis. We selected genes which highly correlated with drug efficacy in the expression levels ($p<0.01$) in both array screenings. A total of 20 genes among 359 candidates satisfied the selection criteria, and 9 genes were finally selected as the most potent markers of sensitivity to 4 drugs after the confirmation of correlations by real-time RT-PCR ($p<0.1$). They were *B4GALT5* (UDP-Gal: ßGlcNAc ß 1,4-galactosyl-transferase, polypeptide 5 gene), *UGCG* (UDP-glucose ceramide glucosyltransferase gene), and *XBP1* (X-box binding protein 1 gene) for 5-FU, *NRCAM* (neuronal cell adhesion molecule gene) for DOX, *ARFRP1* (ADP-ribosylation factor related protein 1 gene), *IFITM1* (interferon induced trans-membrane protein 1 gene), *KIAA0685*, and *SIPA1L2* (signal-induced proliferation-associated 1 like 2 gene) for CDDP, and *CALU* (calumenin gene) for CPT-11 (Table IB). Despite the relatively increased number of potent marker genes, no possible marker genes of MMC-, TXL-, TXT-, or additionally SN-38-induced cytotoxicity were revealed in this approach.

Prediction formulae of sensitivity to 4 drugs in vitro. Selection of the truly significant genes for sensitivities to drugs would allow us to predict therapeutic response to these agents simultaneously, at which point we could understand their interplay in the expression. We therefore attempted to develop such a prediction model using expression data of the selected genes, and performed multiple regression analysis to understand the interplay in the expression of the genes.

Table II. Explanatory variables (x_{ip}) and estimated coefficients (θ_p) in *in vitro* prediction formulae for drug-induced cytotoxicity.

A) Prediction formulae using 5 functionally known genes.

	θ_p				
x_{ip}	5-FU	DOX	CDDP	CPT-11	SN-38
ln [*BCL2*]	0.071	0.159	-0.468	0.086	0.139
	(0.300)	(0.015)	(0.001)	(0.041)	(0.380)
ln [*DPYD*]	0.108	0.029	-0.032	0.007	0.036
	(0.000)[b]	(0.039)	(0.316)	(0.404)	(0.277)
ln [*GSTP1*]	0.138	-0.036	-0.325	-0.052	-0.221
	(0.057)	(0.576)	(0.026)	(0.217)	(0.163)
ln [*MGMT*]	-0.000[a]	0.012	0.022	0.002	0.046
	(0.849)	(0.006)	(0.022)	(0.382)	(0.000)[b]
ln [*XRCC1*]	-0.115	-0.104	0.066	0.215	0.390
	(0.249)	(0.256)	(0.762)	(0.001)	(0.091)
ε_i	5.730	3.724	6.125	7.793	2.394

B) Prediction formulae using 9 highly correlative genes.

	θ_p				
X_{ip}	5-FU	DOX	CDDP	CPT-11	SN-38
ln [*ARFRP1*]	-0.237	-0.127	0.712	-0.213	
	(0.101)	(0.305)	(0.006)	(0.005)	
ln [*B4GALT5*]	0.352	0.065	-0.231	-0.035	
	(0.064)	(0.661)	(0.580)	(0.675)	
ln [*CALU*]	-0.258	-0.075	-0.347	0.178	
	(0.215)	(0.676)	(0.314)	(0.082)	
ln [*IFITM1*]	-0.165	-0.058	-0.274	-0.016	
	(0.030)	(0.341)	(0.043)	(0.649)	
ln [*KIAA0685*]	0.294	0.366	-0.708	-0.016	
	(0.342)	(0.192)	(0.221)	(0.918)	
ln [*NRCAM*]	0.087	0.145	-0.045	0.046	
	(0.052)	(0.000)[b]	(0.565)	(0.027)	
ln [*SIPA1L2*]	-0.044	-0.090	0.039	0.041	
	(0.436)	(0.051)	(0.758)	(0.120)	
ln [*UGCG*]	0.470	-0.081	-0.164	0.145	
	(0.030)	(0.631)	(0.678)	(0.152)	
ln [*XBP1*]	0.087	-0.068	0.864	-0.254	
	(0.676)	(0.679)	(0.038)	(0.012)	
ε_i	5.243	3.745	5.518	8.158	

[ ], expression level of indicated gene; [a]-0.000: -0.0008852; ( ), p-value; [b]0.000: <0.0005.

The expression levels of the selected genes quantified by real-time RT-PCR and cellular sensitivity to drugs (IC_{50} value for each drug) were used as the explanatory variables ($x_1, x_2, \cdots, x_p$) and the response variable (y), respectively, and we estimated ($\theta_1, \cdots, \theta_p$) of the formula in the linear model: $y_i = x_{i1}\theta_1 + x_{i2}\theta_2 + \cdots + x_{ip}\theta_p + \varepsilon_i$ ($i = 1, 2, \cdots, n$), where ε_i is a random error, using NLReg software.